An EP Journal on Architectural Education

Volume No. 12

Issue No. 1

January - April 2024

ENRICHED PUBLICATIONS PVT. LTD

S-9, IInd FLOOR, MLU POCKET,
MANISH ABHINAV PLAZA-II, ABOVE FEDERAL BANK,
PLOT NO-5, SECTOR-5, DWARKA, NEW DELHI, INDIA-110075,
PHONE: - + (91)-(11)-47026006

An EP Journal on Architectural Education

Aims and Scope

An EP Journal on Architectural Education is a National Journal. It Publishes Original Research Papers in Different Areas of Architecture Education. It Publishes 3 Issues in a Year from 2018 in purpose of enhancing architectural scholarship in design, history, urbanism, cultural studies, technology, theory, and practice.

An EP Journal on Architectural Education

An EP Journal on Architectural Education

(Volume No. 12, Issue No. 1, January - April 2024)

Contents

Comparison Of Boundary Shear Stress Along Different Reaches Of A Meandering Channel

Deepika P. Palai[1], K.C.Patra[2], Abinash Mohanta[3]
[1]Civil Engineering Dept., N.I.T. Rourkela, Odisha-769008
India. Email: dpalai22@gmail.com
[2]Professor, Civil Engineering Dept., N.I.T. Rourkela, Odisha-769008
India. Email: kcpatra@nitrkl.ac.in
[3]Civil Engineering Dept., N.I.T. Rourkela, Odisha-769008
India. Email: abinash4435@gmail.com

A B S T R A C T

River meandering is a complicated process involving the interaction of flow through channel bends, bank erosion and sediment transport. Hence the meander formation in rivers is a complicated phenomenon that results from erosion on outer bank and deposition on the inner side. For analysis of meandering channels under different geometric and hydraulic condition are necessary to recognize one of the flow properties such as distribution of boundary shear which is a better indicator of secondary flows than velocity, on different parameters like aspect ratio, sinuosity, ratio of minimum radius of curvature to width and hydraulic parameter such as relative depth. Boundary shear stress being the tangential element of the hydrodynamic forces performing along the channel bed, boundary shear force is evaluated for the bed and side wall of the channel. The distribution of boundary shear force along the wetted perimeter directly affects the flow structure to quantify the momentum transfer along the expected interfaces. Hence the distribution of shear force between the channel bed, inner and outer walls are analyzed for the complete meander path. This is also helpful to evaluate the stage discharge relationship for a meandering channel more accurately.
In this paper, the present research work utilizes the flume facility available in the Fluid Mechanics and Hydraulic Engineering Laboratory of the Civil Engineering Department at the National Institute of Technology, Rourkela, to compute the shear stress distribution along the bed and side walls along a meandering path which is ranging from one bend apex to the next bend apex which changes its course at the crossover. The results of the boundary shear distribution; along the bed, inner wall and outer wall are represented, which would give information about the shear force sharing among them. As the longitudinal velocity remains higher in the inner wall than at the outer wall, hence the shear force would be higher on the inner wall. As the meandering path changes its course, the shear force subsequently changes. Therefore, these features can be considered by the engineers and researchers in the field of interaction losses, sediment erosion, deposition etc.
Keywords—Boundary shear stress, bend apex, crossover, meander path.

1. INTRODUCTION

Water is one of the prime factors which is responsible for life on the earth. Rivers are dependably wondrous things and the historic livelihood of a habitation. Individuals have been living close to the banks of rivers for quite a long time for the enthusiasm of nourishment, water and transport. However, flooding in rivers has always been danger for mankind as this causes a huge loss of property and lives. Moreover, the frequency of occurrence of floods has increased recently due to result of climate change, excessive human intervention, growing population on the banks of rivers and industrialization. Hence it is essential to take measures to understand flooding situations by analyzing the physics behind it.

Generally, river engineer's to use the water powered model to make a flood prediction. River meandering is an entangled methodology which includes the collaboration of move through channel twists, bank disintegration, and silt transport. In rivers, theme and are wind development is an unpredictable wonder that results from erosion on the external bank and deposition on the inner side. So the investigation of meandering channels under different geometric and hydraulic condition is necessary to understand the flow properties, for example, distribution of velocity and boundary shear, which are better indicators of secondary flows, with the variation of different parameters like aspect ratio, sinuosity, ratio of minimum radius of curvature of width and hydraulic parameter such as relative depth and aspect ratio. Water flowing in an open channel is restricted by resistance from the bed and side slopes of the channel. This resistance force is actually the boundary shear force. Boundary shear stress is the tangential component of the hydrodynamic forces acting along the channel bed. The flow attributes of an open channel flow are straightforwardly subject to the boundary shear force distribution along the wetted perimeter of the channel. Exact estimation of boundary shear force distribution is necessary to manage with different hydraulic problems, for example, channel design, channel migration and interaction losses. Bed shear forces are valuable in the investigation of bed load transfer where as wall shear forces present a general view of the channel migration pattern. Rajaratnam and Ahmadi (1981) demonstrated that the boundary shear stress reduces from the center of the meandering channel toward the edge of the meandering channel. Then it roughly increases at the interface with the edges, subsequently it decreases and levels off for most of the width and finally decreases near the wall. They have also done that the effect of the meandering channel is to reduce the boundary shear stress. Shear stress is highly affected by the secondary currents while according to Knight and Demetriou (1983), it increases where the secondary currents flow in the direction of the wall and decreases when they flew away from the wall.

2. Experiment Setup

Evaluation of discharge capacity of a meandering channel is a complicated process due to various factors such as the geometry of channel, types of channel and patterns of channel, channel roughness and sediment concentration. It is directly dependent on accurate predictions of velocity distribution in the meandering channel. Velocity distribution is never uniform across a cross-section of meandering channel. It is higher in the deeper main channel than the shallower floodplain, as in compound channels the shallow flood plains offer more resistance to flow than a deeper main channel. The present research work utilizes the flume facility available in the Fluid Mechanics and Hydraulic Engineering Laboratory of the Civil Engineering Department at the National Institute of Technology, Rourkela, India. The objective behind the experiment is to get a better understanding of stage discharge and the boundary shear stress distribution along the bed and side walls in a meandering path which is ranging from one bend apex to the next bend apex which changes its course at the crossover. The following section provides a brief overview of details of hydraulic and geometric parameters of the present meandering

process. Water is supplied through a Centrifugal pump (15 HP) discharging into an RCC overhead tank. There will be a measuring tank present in downstream end, followed by a sump which will feed to overhead tank through pumping thus completing the recirculation path. The Figure 1 represent the schematic diagram of the experimental setup of Meandering Channel. Water was supplied to the flume from an underground sump via an overhead tank by centrifugal pump (15 hp) and recirculation to the sump after flowing through the compound channel and a downstream volumetric tank fitted with closure valves for calibration purpose .Water entered the channel bell mouth section via an upstream rectangular notch specifically built to measure discharge in the experimental channel. An adjustable vertical gate along with flow strengtheners was provided in upstream section sufficiently ahead of rectangular notch to reduce turbulence and velocity of approach in the flow near the notch section. At the downstream end another and maintain a uniform flow in the channel. The movable bridge was provided across the flume for both span wise and stream wise movements over the channel area so that each location on the plan of meandering channel could be accessed for taking measurements.

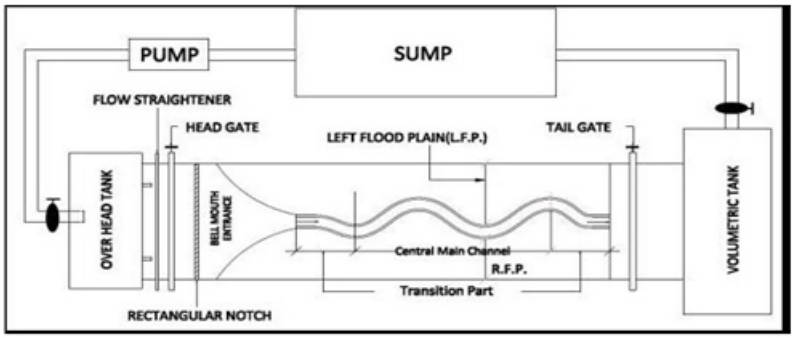

Figure 1 Experimental Setup of Meandering Channel

2.1. Channel Description

Sl.no	***Description***	***Types***
1	*Type of Channel*	*Meandering channel*
2	*Flume Size*	*(14*1.5*0.3)*
3	*Meandering Channel Geometry*	*Rectangular*
4	*Type of Bed Surface*	*Smooth*
5	*Section of Channel*	*0.25m*
6	*Bank Full Depth*	*0.12m*
7	*Meandering Angle*	*60°*
8	*Width Of Main Channel Section*	*0.28m*
9	*Bed Slope Of Main Channel*	*0.0006*
10	*Top Width Of Compound Channel*	*1.67m*
11	*Type Of Flood Plain*	*Symmetric*
12	*Wave Length (L)*	*2.23*
13	*Amplitude (A)*	*1.13*
14	*Sinuosity*	*2.04*
15	*Aspect Ratio* (δ)	*2.434*

Table: 1 Details of experimental parameters for meandering channel

3. STAGE- DISCHARGE RELATIONSHIP

Making a flood predictio while using a hydraulic model which incorporates various flow features, is not an easy task. Researchers have shown that the structures of the flow are even more difficult to analyze for meandering channel, due to an increase in the 3-Dimensional nature of flow (Shiono, Al-Romaih, and Knight 1999). In the present experimentation involving flow in a meandering channel, steady and uniform flow has been trying to achieve. Flow depths in the experimental channel runs are maintained that the water surface slope becomes parallel to the valley slope to minimize the energy losses. Under such conditions, the depths of flow at the channel centerline along one wave reach must be the same. This depth of flow is considered as normal depth, which can carry a particular flow only steady and uniform condition. Figure.2 represent the graph of a stage discharge relationship in a main channel of a meandering channel.

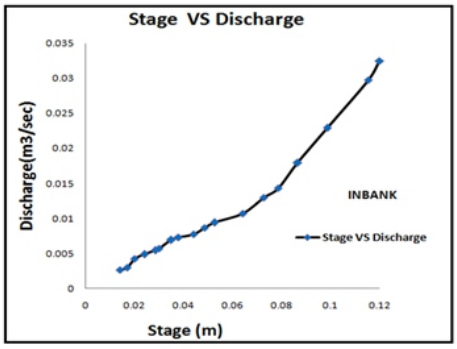

Figure.2 graph of a stage discharge relationship in a main channel of a meandering channel.

4. BOUNDARY SHEAR STRESS

When water flows in a channel the force developed in the flow direction is resisted by the reaction from channel bed and side walls. This resistive force is manifested in the form of boundary shear force. The distribution of boundary shear force along the wetted perimeter directly affects the flow structure in an open channel. Understanding of boundary shear stress distribution is necessary to define the velocity profile and fluid field. Also, computation of bed form resistance, sediment transport, side wall correction, cavitations, channel migration, conveyance estimation and dispersion are among the hydraulic problems which can be solved by bearing the idea of boundary shear stress distribution. From hypothetical considerations, in steady, uniform flow in the boundary shear stress is related to channel bed slope, hydraulic radius and unit weight of fluid. Tominaga et al.(1989)and Knight and Demetriou (1983)declared that boundary shear stress increases where secondary currents flow towards the wall and shear stress decreases as they flow away from the wall. The presence of the secondary flow cells in the main flow influences the distribution of shear stress along the channel wetted perimeter. In In meandering channels the factors increases by many folds due to growth in 3-Dimensional nature of the flow. Sinuosity of meandering channel is considered to be a critical parameter for calculating the percentage of shear force at channel walls and bed.

5. MEASUREMENT OF BOUNDARY SHEAR STRESS

Estimation of shear stress in open channel flow helps in comprehension shear bed load transport, momentum transfer, channel migration; etc. The shear forces at the bed are advantageous in the examination of bed load transfer whereas shear forces at the walls give a general survey of the channel migration pattern. Although there are a few systems, methods to evaluate bed and wall shear, the Preston - tube method being an indirect estimate, is broadly utilized for experimental observations.

Preston (1954) added to a fundamental methodology for measuring local shear stress on smooth boundaries utilizing a Pitot tube in contact with the surface. His system was based on the assumption of an inner law relating the boundary shear stress to the velocity distribution near the wall. Preston showed a non-dimensional relationship between the Preston tube differential pressure ΔP, and the limit shear stress (τ) of the form:

$$\left(\frac{\tau d^2}{4\rho v^2}\right) = F\left(\frac{\Delta P d^2}{4\rho v^2}\right) \quad (1)$$

Where d is the external diameter of the Preston tube, ρ is the density of the flow, υ is the kinematic viscosity of the fluid and F is an empirical function. Patel (1965) further extended the research and his adjustment is given about of two non-dimensional parameters x* and y* which are utilized to change over pressure readings to boundary shear stress, where

$$x^* = \log_{10}\left(\frac{\Delta P d^2}{4\rho v^2}\right) \text{ and } y^* = \log_{10}\left(\frac{\tau d^2}{4\rho v^2}\right) \quad (2)$$

In the form

For $y^*<1.5$ $\quad y^*=0.5x^*+0.037$ (3)

For $1.5<y^*<3.5$ $\quad y^*=0.8287-0.1381x^*+0.1437x^{*2}-0.006x^{*3}$ (4)

And

For $3.5<y^*<5.3$ $\quad x^* = y^* + 2\log_{10}(1.95y^* + 4.10)$ (5)

In the present case, all shear stress estimations are taken at all the thirteen sections through the meander path between the two bend apexes. The pressure readings were taken utilizing pitot tube along the predefined points over all the portions purposes of the channel along the bed and side slopes. The manometer is attached to the Pitot tube which gives the head distinction between the dynamic and static pressures. Then the differential pressure is calculated from the readings on the vertical manometer by,

$$\Delta P = \rho g \Delta h \quad (6)$$

Where Δh is the distinction between the two readings from the dynamic and static, g is the acceleration due to gravity and ρ is the density of water. Here the tube coefficient is taken as a unit and the error due to turbulence is considered negligible while measuring velocity.

Accordingly, out of the Eq. 2-6, the appropriate one was chosen for processing computing the wall shear stress based on the range of x* values. After that the shear stress value was facilitated over the whole perimeter to calculate the aggregate shear force per unit length normal to flow cross-section carried by the meandering section. The total shear in this way computed was then contrasted with the resolved component of weight force of the liquid along the flow-wise direction to check the accuracy of the measurements.

6. DISTRIBUTION OF BOUNDARY SHEAR STRESS RESULTS

Shear stress distribution along the cross section of the channel is required to find out to know the variation of shear stress along the bed and it is also helpful in finding out the apparent shear stress in the channel section. In general Patel's equation is used to find out the shear stress develop at the bed and wall of the channel. Boundary shear stress at the bed and wall of the main channel at bend apex and crossover are presented in the figure 3 and figure 4 of aspect ratio(α)=2.54. Similarly the figure 5 and figure 6 are represented the bend apex and crossover of aspect ratio (α)=9.33 respectively.

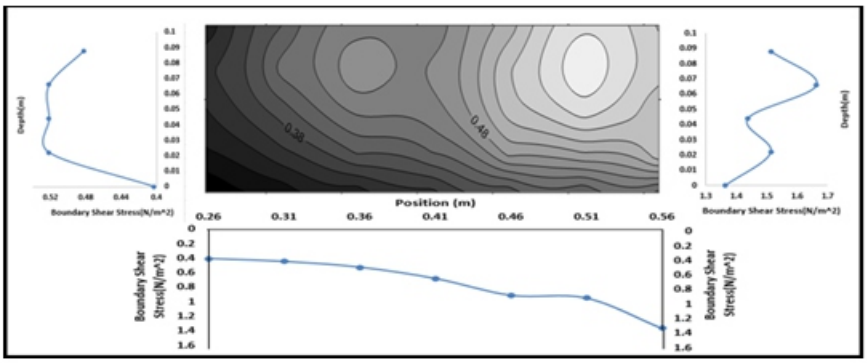

Figure 3 Boundary shear stress at the bend apex at α=2.54

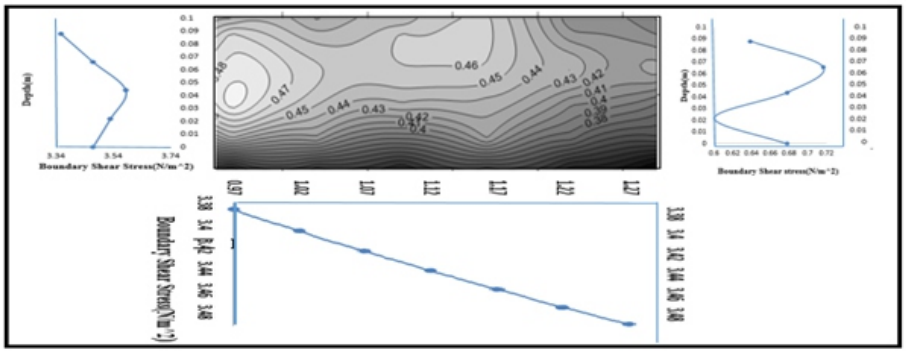

Figure 4 Boundary shear stress at crossover at α=2.54

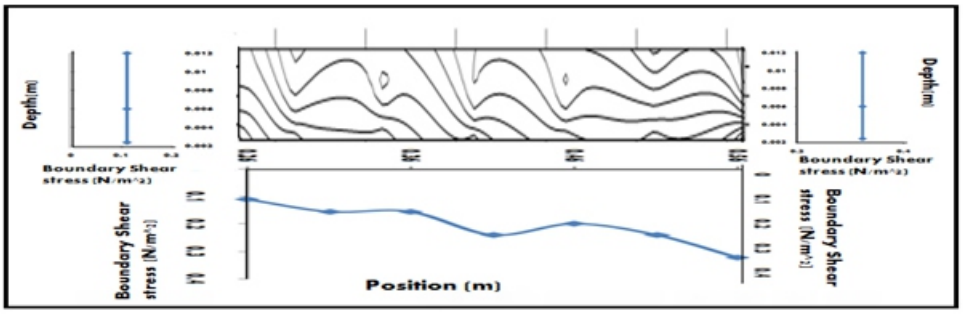

Figure 5 Boundary shear stress at the bend apex at α=9.33

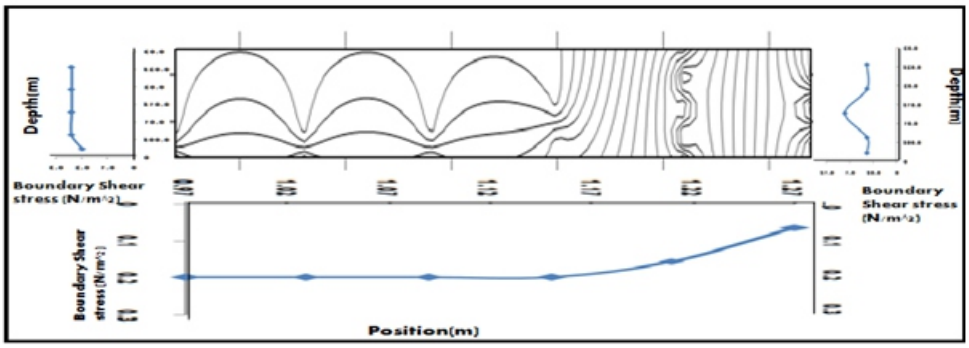

Figure 6 Boundary shear stress at crossover at α=9.33

7. RESULTS AND DISCUSSIONS

Boundary shear measurements are carried out at different sections from one bend apex to another bend apex during the cross-over. Here also boundary shear measurements are carried out bend apex and cross-over in a meander path. The figure 3, 4, 5 and 6 illustrates the boundary shear stress distributions across the channel bed and the side slopes at the inner and outer walls for bend apex and cross-over reaches of measurement.

1. The shear stress profiles along the surface of the channel are represented by viewing the stress curves perpendicular to all the three sides of the channel; namely the bed, the inner wall and the outer wall. Hence the figures give a clear demonstration about the boundary shear stress distribution throughout the channel section.

2. The distribution of boundary shear stress along the wetted perimeter in meandering channels follows sinusoidal (non-uniform) pattern. The distributions of boundary shear stress are used to highlight secondary flow currents, as the boundary stress is usually a better indicator of their presence than isovel patterns (Knight and Patel, 1985).

8. CONCLUSIONS

Experiments are carried out to investigate the effect of sinuosity and channel aspect ratio on the boundary shear in a meandering channel. Point to point observations are made at bend apex of meandering channel for wall shear data at different aspect ratio (α) are 2.54 and 9.33 respectively of the meandering channel. Based on analysis and discussions of the experimental investigations certain conclusions from the present work are as discussed underneath:

1. It is also observed in case of simple meandering channel that, as the aspect ratio in the main channel decreases the ratio of shear force between the inner and outer walls increase indicating that the shear force per unit length at inner wall increases faster with respect to the outer walls. Similarly, it can be seen that though the bed and wall shear increases with depth of flow in main channel, the rate of increase in wall shear is nearly four times the rate of increase in bed shear giving rise drastic decrease in the ratio of bed to wall shear with decrease in aspect ratio.

2. The boundary shear stress distribution at the cross-over sections is found to be more or less uniform throughout the channel section.

3. The sinusoidal distribution of boundary shear stress along the wetted perimeter is observed which confirms the presence of secondary currents in meandering in bank flows.

4. From the results of Shear stress measurements it is found that the shear stress at the inner wall always remains higher as compared to that at outer wall.

REFERENCES

Khatua, K.K. and Patra, K.C. (2010). Evaluation of boundary shear distribution in a meandering channel. Proceedings of ninth International Conference on Hydro-Scienceand Engineering, IIT Madras, Chennai, India, ICHE 2010, 74.

Knight, D. W. (1981). Boundary shear in smooth and rough channels. J. Hydraul. Div., Am. Soc. Civ. Eng., 107(7), 839–851.

Patel, V.C. (1965). Calibration of the Preston tube and limitations on its use in pressure gradients. Journal of Fluid Mechanics, 23(01), 185-208.

Preston, J. (1954). The determination of turbulent skin friction by means of Pitot tubes. Journal of the Royal Aeronautical Society, 58(518), 109-121.

Rajaratnam, N., and Ahmadi, R.M. (1979). Interaction between Main Channel and Flood Plain Flows. Journal of Hydraulic Division, ASCE,105(5), 573-588.

Rhodes, D. G., and Knight, D. W. (1994). Distribution of Shear Force on Boundary of Smooth Rectangular Duct. Journal of Hydralic Engg. , 120-7, 787– 807.

Saine S. Dash, K. K. Khatua, P. K Mohanty (2013). Energy loss for a highly Meandering open Channel Flow. Res. J. Engineering Sci.,2(4), 22-27.

Saine S. Dash, K. K. Khatua, P. K. Mohanty (2013). Factors influencing the prediction of resistance in a meandering channel. International Journal of Scientific & Engineering Research , 5(4).

Sellin R. H. J. (1961.). A Study of the Interaction between Flow in the Channel of a River and that over its Floodplain. Ph. D Thesis, University of Bristol, Bristol, England

Sellin, R. H. J. (1964). A Laboratory Investigation into the Interaction between the Flow in the Channel of a River and that over its Floodplain.La. Houille Blanche.

Shiono K., Al-Romaih I. S., and Knight D. W., (1999). Stage-discharge assessment in compound meandering channels. Journal of Hydraulic Engineering, ASCE, 125 (1), 66- 77, Mar., 45-54, and discussion in 1993, 101, 251-252.

Depth-Averaged Velocity Distribution for Meandering Compound Channel

Saine S. Dash[1], Kishanjit K. Khatua[2],Subhasish Dey[3]
[1]Ph.D Scholar, Dept. of Civil Engineering, National Institute of Technology, Rourkela-769008, India
[2]Associate Professor, Dept. of Civil Engineering, National Institute of Technology, Rourkela-769008, India
[3]Professor and Brahmaputra Chair, Dept. of Civil Engineering, Indian Institute of Technology, Kharagpur 721302, West Bengal,India
Email: sainedash@gmail.com

ABSTRACT

Prediction of flow and velocity distribution along the river cross section is essential in many hydraulic engineering studies involving bank protection, sediment transport, conveyance, water intakes and geomorphologic investigation. It is quite difficult to model flows in meandering trapezoidal compound channel that exerts unequal shear drag on the fluid flow that ultimately controls the depth averaged velocity. The discharge prediction in meandering compound channels is usually assessed relating, with some adjustments, the same methods used in the straight compound channels. Specifically, the sinuosity of the main channel is frequently introduced to account for its meandering pattern, although some methods use different geometric parameters.Some methods and formulae have been proposed in the literature to estimate the depth average velocity for meandering compound channels. Flow structure in meandering channels is more complex than that of straight channels due to the energy dissipations caused by the development of strong secondary currents. Due to the effect of secondary currents, it makes difficult to computation of the depth-averaged velocity in meandering compound channels. For the complex flow phenomenon occurring in a meandering compound channel, Depth Averaged Velocity is not symmetrical and depends upon many non-dimensional hydraulic and geometric parameters.This paper presents a practical method to predict lateral depth-averaged velocity distribution in trapezoidal meandering compound channels by using different numerical software such as 2D CCHE2D and 1D CES.

Keywords—Depth Average Velocity, MeanderingCompound Channel, Sinuosity, Flow Depth, Secondary Current.

1. INTRODUCTION

Throughout ancient and modern times, water has been crucial to humankind as an essential source for life. This is why human beings settled on the floodplains or coasts, despite the risk of periodic flooding. In fact, these regions attracted mankind because of the advantages and benefits related to soil fertility for agriculture, the availability of water for different uses, and transportation. This is crucial for both survival and for reducing any threat. The Flood predictionwas a vital part of engineering work, and they also require the conveyance capacity and depth average velocity distribution for a given flood event. These parameters are important in generating the stage-discharge curve, which is often extrapolated to estimate the water level for a given frequency of flow. Such estimates are also required in engineering problems to do with bank protection, sediment transport and scour analysis. The flow simulation in a compound channel during a flood event is complicated due to the nature of the flow. This is surprising,

since natural channels are irregular in shape, and often consist of a deep channel with adjacent flood plain(s). Because of the lateral and vertical momentum transfer between the different depths, the flow conditions in such kinds of channel are more complex than those in a simple channel. Owing to the importance of such channels in the natural environment, a better understanding of flow in complex channels is vital, and a scientific necessity. As a result, the prediction of the above stated parameters in a two-stage meandering channel is difficult. In fact, the difference in velocity between the faster moving water in the main channel and the slower moving water in the floodplain results in the creation of vortices in which high lateral exchanges of momentum take place. In addition to the vorticity generated along vertical axes, secondary flows in the longitudinal streamwise direction also may take place. This longitudinal vortices is present in the turbulent flows in non-circular sections, which is the case for open channel. The depth average velocity decreases with the distance moved from the river channel to the floodplain. The prediction of the depth average velocity in meandering compound channels is a challenging task for rivers engineers due to the nature of flow. The dominant feature consists of the interaction effect between the fast moving flow in the main channel and the slow co- flowing flow on the floodplains. This results in a high shear layer at the interface between the main channel and floodplain, leading to the generation of large-scale vortices with vertical axes, and depth-scale vortices with longitudinal axes, Tominaga & Nezu (1991). The depth averaged velocity data collected from experimentation with sinuosity 1.11 . For different depth of flow tha data analysed and validate with different numerical models such as CCHE2D and CES.

2. PREVIOUS INVESTIGATIONS

The Basic Concepts for velocity recognised as early as the mid 1800s when Moseley (1872), Francis (1879), Wood (1879), Cunningham (1882), Stearns (1883) and others undertook work to establish why the maximum velocity in open channels occurred below the surface.Prandtl (1964) is generally credited with analysing secondary flow. Prandtl's secondary flow of the first kind, (Liggett et al. (1965) "strong" currents) arises due to centripetal forces caused by bends or changes in cross-sectional area. This is not directly related to turbulence, therefore it will not be examined any further.Gerard (1978) pioneered an approach which enables the prediction of secondary flow streamlines.Shiono and Knight (1988) to develop an analytical approach longitudinal streamwise momentum equation in conjunction with a depth averaged eddy viscosity, they were able to predict the mean velocity.Tominaga et al. (1989) have successfully modified Gerard's approach. The velocity gradient of the secondary flow also affects the lateral distribution (Knight and Shiono, 1996) and pattern of isovels (Knight and Patel, 1985). Nezu et al. (1993) conducted a measurement of secondary flow in a man-made river with a river width and depth values of 17.5m and 2.2m respectively and interpreted several sets of secondary cells along the river.

Ervine, et al. (1993) reported that the interaction between floodplain and main channel flow in such conditions will generate a large scale secondary cell, which grows in width along the cross-over length and then decays rapidly. In relation to this, Shiono and Muto (1998) reported that the floodplain flow tends to be more tangential to the main channel flow with increasing relative depth and the streamlines of water surface were almost wholly aligned with longitudinal direction.Willets and Rameshwaran (1996) conducted laboratory experiments to determine the flow structures present in a meandering two-stage channel and suggested that this increase caused less energy dissipation at the interface between the floodplain and the main channel. This suggestion was supported by an increase in the magnitude of the secondary flow circulation in the trapezoidal channel than in the natural channel. It was also reported that the location of the maximum streamwise velocity relocated to the inner meander bend with rising water depth.

3.EXPERIMENTAL SETUP

The series of experiments were carried out using the Tilting Flume research facility at Hydraulics Laboratory of NIT Rourkela.An experimental investigation has been carried out on the effect of various channel geometry parameters on the interaction mechanism which exists between a channel and its associated flood plain during overbank flow. Measurements were conducted in a 15 m long perspex titling flume in the Hydraulics Laboratory of NIT Rourkela. Figure 1 shows a cross-section of that flume and Figure2experimental setup of compound meandering channel.The water is pumped from wide outlet tank through a castiron circular pipe and into an inlet tank upstream from which the water flows into the flume. The flume has an adjustable bed slope S_0 which was set to 0.0011so that water could flow in the inside channels under gravity.To minimize the effects of inlet turbulence on flow development, one0.395 m long by 1.5m highmesh with small uniform holes were placed at the inlet to straighten the flow and reduce the disturbances due to inlet turbulence. The flume is a trapezodial meandering compound channel. The experimental channel was built inside the existing walls of the flume with Perspex sheet (6 to 10 mm thick) is used for the bed and wall of channel thick having Manning's n value=0.01. The flume is 15m long has a main channel width of B_{mc} = 0.33 m and a floodplain width of B_{fp} = 0.395 m. The Pitot tube is a pressure instrument to measure longitudinal fluid flow velocity.The main purpose of the experiments carried out in this study is to obtain isovels and depth-averaged velocity profiles. The L-shaped Pitot tube used in this study has an inner tube diameter of 4.77 mm and placed perpendicular to the flow.In order to investigate the depth average velocity in meandering compound channel, a series of experiments were undertaken using the Pitot tube. In addition, point velocities were measured across the whole cross-section for selected flow depths. Moreover, the interaction between the main channel and flood plain of a compound channel is also of particular

compound channel, Sinuosity, S_r=1.11 was chosen as the centerline of the path for the main channel as sine generated curves closely approximated the shape of real river meanders whereas the floodplains were made to run straight thus mimicking a natural river flanked by unsymmetrical adjoining floodplains on either side.

Table-1: Details of Geometrical Parameters of the Meandering Compound Channel

Sl.No.	Descriptions	Meandering compound channel
1	Type of main channel	Trapezoidal
2	Main channel bottom width (2b)	33cm
3	Bank full Depth of main channel	65mm
4	Top width of compound section (2B)	395cm
5	Side slope of main channel	1V:1H
6	Bed slope of the channel (S)	0.0011
7	Sinuosity (Sr)	1.11
8	Type of floodplains	Unsymmetrical
9	Flume size (l×b×h)	15m×4m×0.5m
10	Type of main channel	Trapezoidal

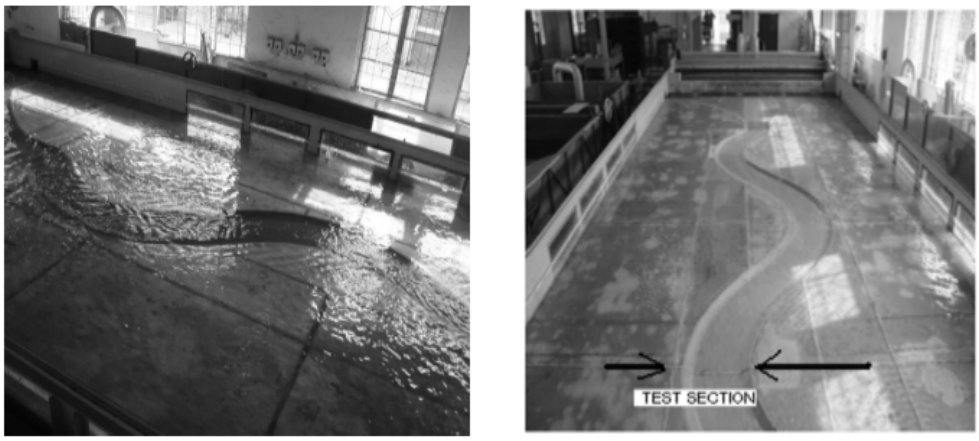

Figure 1. Photographs of the Experimental Channel

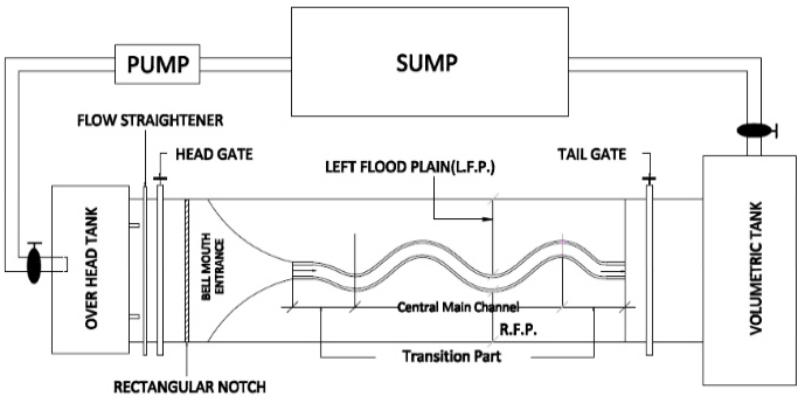

Figure 2.Experimental Setup of Meandering Compound Channel

4.RESULTS AND DISCUSSIONS

In meandering compound channel, the depth average velocity (U_d) are measured for five depth of flow. Depth average velocity normalised with sectional mean velocity for non-dimenssional. All the depth average distribution graphs are presented in Fig 3 for different depth of flow. From fig 3 clearly seen that, in the left floodplain,the curve rising steep from far end near the inner wall of the bend and then it has sharp fall across the width of only main channel. In case of right floodplain the depth average velocity gradually fall towards the end of the floodplain. In the low depth of flow , it clearly visible that the trend is more prominent and in higher depth of flow comparatively is very less. The maximun depth average velocity occurs over the inner wall of the bend which is about two times of mean velocity and 10% more than the mean velocity in higher depth of flow cases.

Here the experimental research undertaken two numerical hydrodynamic tools viz. Conveyance Estimation System (CES) and CCHE2D are applied to simulate the depth average velocity for diiferent depth of flow cases for meandering compound channels. CCHE2D is 2D and CES is 1D numerical hydrodynamics software tood developed by respectively NCCHE, USA and HR Wallingford, UK. CCHE is an integrated system which is composed of a Graphical Users Interface (CCHE-GUI), a separate hydrodynamic numerical model (CCHE2D model) and a structured mesh generator (CCHE2D Mesh Generator).Depth averaged velocity are extracted numerically from simulation results and compaired with experimental datas. By using numerical analysis such as CES and CCHE2D the depth averaged velocity calculated and compared with experimental datas.in fig 3 and 4 shows depth averaged velocity normalised with maximum velocity among all the three i.e. Experimental, CES and CCHE2D respectively for meandering compound channel. In meandering compound channel, the depth averaged velocity output shows in fig 4 (i-v). from graph clearly observed that, CCHE2D prediction gives good results with experimental datas. CES also matched with CCHE2D and experimental datas in higher depth of flow (fig 4,iii-v). However, at low depth of flow(fig 4,i & ii) some deviation occurs particularly in main channel region.

From the above simulation seen that CCHE2D are gives depth averaged velocity values quite satisfactory in meandering compound channel with wide floodplains. CES also quite useful in meandering compound channel and both the numerical software have good application in compound channel research work.

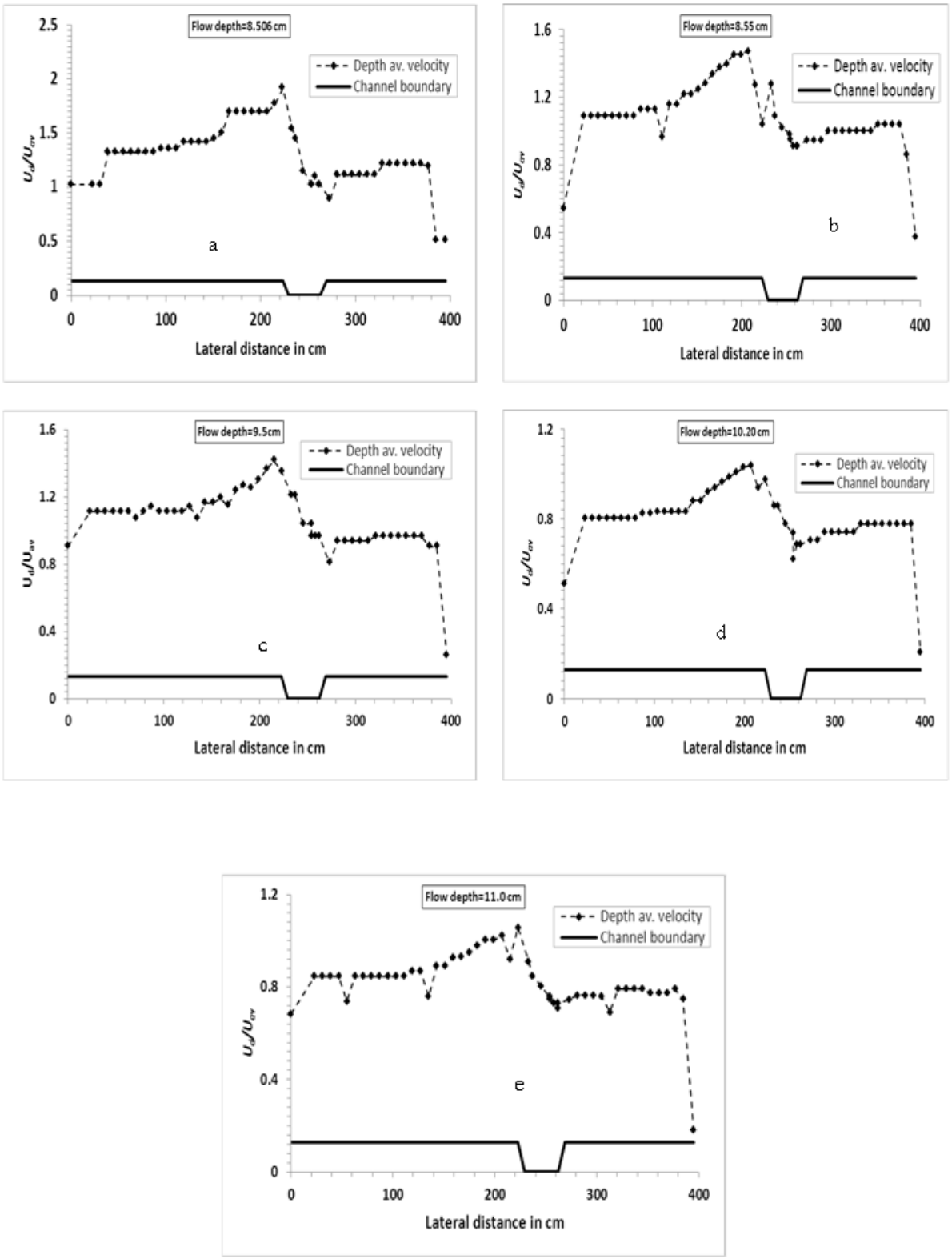

Figure.3 (i-v)Depth averaged velocity distribution (Ud normalized with Uav) for meandering compound channel

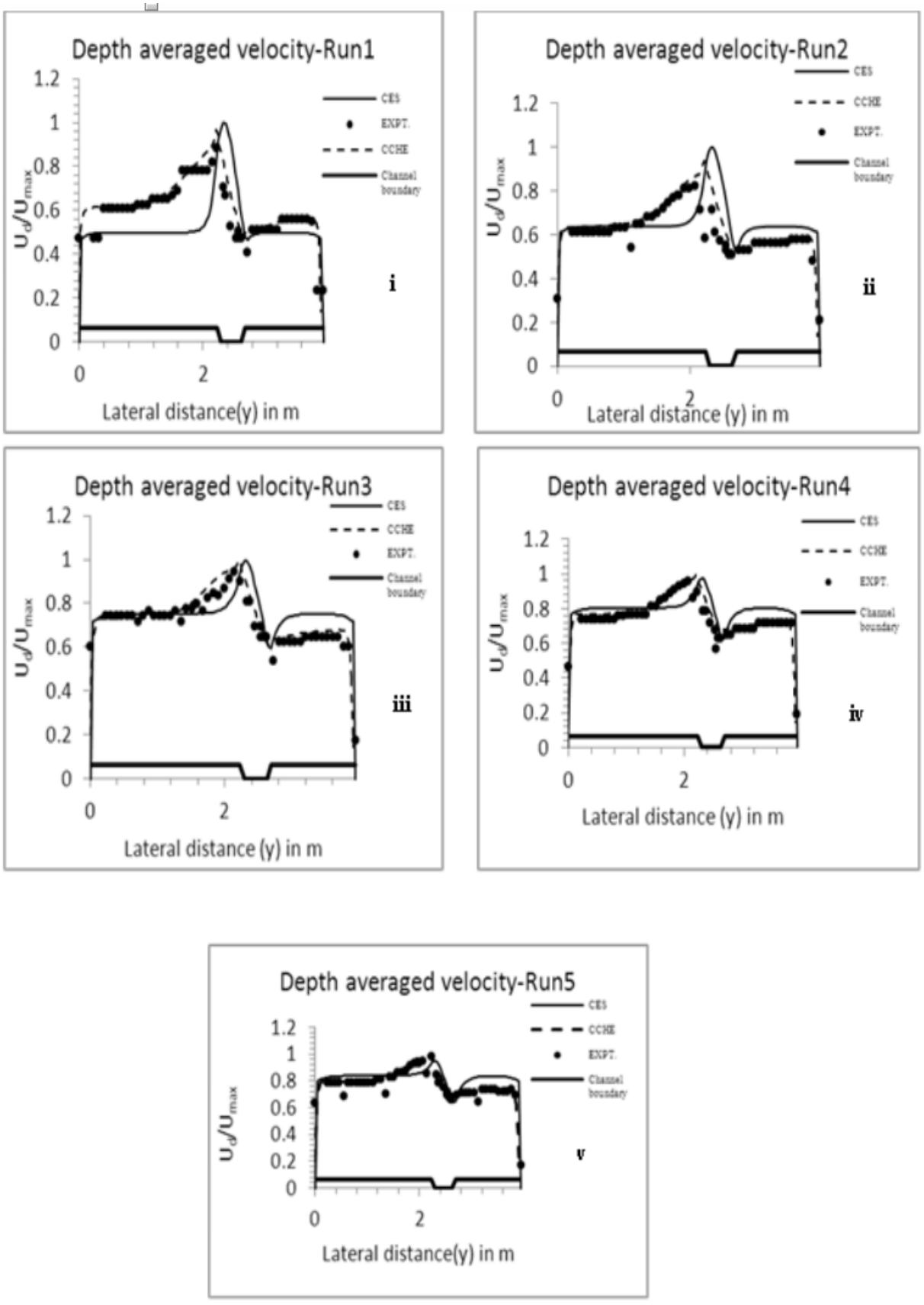

Figure.4 (i-v)Depth averaged velocity (Ud) normalized with Umax for different approaches for different depth of flow

5.CONCLUSIONS

- The depth averaged velocity at the bend apex for different depth of flow have been measured in meandering compound channels.
- The depth averaged velocity distribution in meandering compound channels shows the effect of momentum transfer between main channel and floodplain flow. The momentum transfer is stronger at the lower depth ratio as compared to the higher. The depth averaged velocity distribution in meandering compound channel shows that the maximum depth averaged velocity magnitude is always observed over the inner side of the bend apex. The maximun depth average velocity occurs over the inner wall of the bend which is about two times of mean velocity and 10% more than the mean velocity in higher depth of flow cases.
- A 1D model (CES) and a 2D hydrodynamic model (CCHE2D) have also been applied to calculate the depth averaged velocity of meandering compound channels for different depth of flows. From the numerical analysis the results discussed.
- From 1D model CES is simuated for depth averaged velocity in wide meandering compound channel and observed that this package gives under predicted observed value in most depth of flow cases for meandering compound channels.
- And 2D numerical tools CCHE2D is also applied for meandering compound channel and its gives good results compaired to CES. CCHE2D are gives depth averaged velocity values quite satisfactory in meandering compound channel with wide floodplains.

REFERENCES

Cunningham A (1882), Recent hydraulic experiments, Minutes of proceedings Inst. of civil Eng. London Vol LXXI

Ervine, D.A, Willets, B.B., Sellin, R.H.J. and Lorena, M. (1993), Factors affecting conveyance in meandering compound channel flow, Journal of Hydraulic Engineering, ASCE, Vol. 119, No. 12 December.

Francis, J. B. (1879), on the cause of the maximum velocity of water flowing in open channels being below the surface, Transactions ASCE vol VIII

Gerard, R (1978), Secondary flow in non-circular conduits, J. Hydr div. ASCE Hy5 pp755-773

Knight D W & Patel H S (1985), Boundary shear in smooth rectangular ducts, J Hyd Eng., ASCE, Vol.111, No. 1, pp 29-47

Knight D W &Shiono K (1990), Turbulence measurements in a shear layer region of a compound channel, J Hydr. Res. IAHR, Vol 28, No. 2, pp 175-196

Liggett J. A., Chiu C. L. & Miao L. (1965), Secondary currents in a corner,J.Hydr.Div. ASCE, 91, 6, pp. 99-117

Moseley, H. (1872), on the steady flow of a liquid Philosophical magazine University of London 4th series Vol XLIV.

Noat D, Nezu I & Nakagawa H (1993), Hydrodynamic behaviour of compound rectangular open channel, J.HyrdEng ASCE, Vol 119, No.3, pp 390-408

Prandtl L. (1964), Essentail fluid dynamics, Blackie, 48

Shiono K & Knight D W (1988), two dimensional analytical solution for a compound channel, Proc 3rd Int. Symp on refined flow modelling and turbulence measurements, Tokyo, July pp 503-570

Shiono, K. and Muto, Y. (1998), Complex flow mechanisms in compound meandering channels with overbank flow, J. of Fluid Mechanics, Vol 376, pp 221-261.

Stearns F. P. (1883), on the current meter, together with reasons why the maximum velocity of water flowing in open channels is below the surface, Transactions ASCE Vol XII

TominagaA,Nezu I. (1991), Turbulent structure in compound open channel flows, J.Hydr.Eng., ASCE, Vol. 117, pp 21-41
Tominaga, A., Nezu L, Ezalci, K, &Nakagawra, H (1989), three dimensional structure in straight open channel flow, Journal of hydraulic research IAHR Vo127, pp 149-173
Willetts, B.B. and Rameshwaran, P. (1996), Meandering Overbank Flow Structures. Coherent Flow Structures in Open Channels, Edited by P.J. Ashworth, S.J. Bennett, J.L. Best and S.J. McLelland, Chapter 29, 609–629.
Wood Devolson (1879), on the flow of water in rivers, Transactions ASCE vol VIII, July

Estimation of evapotranspiration based on an Extended Three-Temperature Model and MODIS products in ecosystems of Northeast India

Suman Kumar Padhee[1], Subashisa Dutta[2]
[1]Research Scholar, IIT Guwahati, Guwahati-781039, India
[2]Professor, IIT Guwahati, Guwahati-781039, India
Email**:** suman.iirs@gmail.com

A B S T R A C T

Evapotranspiration (ET) is an essential component critically involved in the energy balance and water budgeting methods, which are in at most use in the current date for estimation of several hydrological parameters. The precise assessments of ET are crucial for developing knowledge in hydrological processes. Traditional methodologies used for ET computation are good for point estimation which offers quantitative analysis, but are limited towards its spatial distribution which delivers qualitative exploration. Here, the inclusion of Remote Sensing data with properties of broad spatial coverage and good spatial, spectral and temporal resolution plays an important role. But still, the computation of ET requires creation of a data rich environment which is itself a big task. Due to the difficulty in determination of aerodynamic, canopy and soil resistance parameters, estimating ET by remote sensing technology for regional applications is a challenge, regardless of growing anxieties. At a macro-scale level, one important approach for the achievement of this goal is accurate estimate of spatially distributed soil evaporation (LE_s), which can be later used to distinguish from transpiration from canopy (LE_c) and their combination will provide the total ET. The 'Extended Three Temperature Model' (Extended 3T Model) along with Moderate Resolution Imaging Spectroradiometer (MODIS) products at 1km spatial resolution is an advanced approach, capable of computation for ET and their partition of evaporation (LE_s) and transpiration (LE_c). A case study was conducted in the states of Arunachal Pradesh and Assam in India for years 2002 – 2007. The extended 3T model was used by including its pre-requisite the land surface temperature (T_s), which was separated into the surface temperature of dry soil (T_{sm}) and the surface temperature of vegetation (T_{cm}), decided upon a derivative of vegetation indices (NDVI and EVI) called as the fractional vegetation cover (f). The separated land surface temperatures for soil and canopy cover were used to calculate the evaporation (LE_s) and transpiration (LE_c) separately. Combination of (LE_s) and (LE_c) generated the total ET. The spatiotemporal variation of ET from NDVI and EVI were analyzed in different ecosystems within the study area.

Keywords—Evapotranspiration, Three-Temperature Model (3T Model), Remote Sensing, Evaporation, Transpiration

1. INTRODUCTION

Evapotranspiration (ET) is an essential component for its energy and mass balance in global ecosystems. Water mass balance is characterized by "runoff and evaporation balance" (Jiang and Liu 2010). The potentiality of processes such as surface energy and water exchange involving ET defines the

environmental characteristics, which makes ET one of the prime focuses. ET is crucial portion to compute water balance and proceed for water management. Hence, ET estimation has been a vital subject in terrestrial ecosystems (Nemani et al. 2002).

Understanding hydrological processes and forming water resources management strategies at global and regional scales require accurate estimates of water budgets (Kite and Droogers 2000). On a global basis, ET accounts for about 70% of total precipitation from the land surface (Rosenberg et al. 1983). Speaking of water loss, about 80% of consumptive water use is lost in ET for global crop production (Liu et al. 2009), and can even range 80–90% in arid and semi-arid areas (Gowda et al. 2008). Such crucial proportion of ET in natural processes and applications explains importance of ET estimation. The methods to estimate ET can be categorized into three groups: water balance method, micrometeorological method and plant physiology method. Since micrometeorological and plant physiology methods face practical difficulty, suitability of these methods are limited to micro scale for homogenous surfaces. Such limitations make ET estimation as one of the most challenging subjects (Mu et al. 2007).

The capability of remote sensing technology to provide surface information has made it possible to estimate surface ET at large scale. Popular algorithms based on thermal remote sensing have been developed, like SEBAL (Surface Energy Balance Algorithm for Land) (Bastiaanssen et al. 1998a and Bastiaanssen et al. 1998b). These algorithms had been suitable for applications in certain places only. But, still most algorithms are inappropriate for practical use because of either rationality of assumptions or unavailability of other supporting data. The most common problem in ET estimation by remote sensing techniques is that the algorithm is generally complex due to contribution of numerous meteorological parameters like aerodynamic resistance, surface resistance etc. Participation of such parameters requires assumptions and site-specific coefficients which are generally complicated to quantify (Li et al. 2005). Moreover, the separation of the parameters evaporation and transpirations is yet to be included in many algorithms which can be considered as a disadvantage. Qiu et al. (1996) and Qiu et al. (1998) proposed an algorithm named the three temperature model (3T model), which overcomes some of the shortcomings.

This study was carried out as an advancement of 3T model followed by Tian et al. (2013) for Brahmaputra River basin, tributaries contributing within India and Bhutan, and consisting of hilly terrain and flood plains where elevation plays an important role in the variation of ET. Spatial and temporal dynamics of ET was determined using extended 3T model during the years 2000 – 2013, and the Moderate Resolution Imaging Spectroradiometer (MODIS) datasets on a basis of 16 days. Also,

quantification of ET was portioned into LEs and LEc for the same period. The variation of ET was discussed for different land covers in the ecoregions within the basin as a comparison between estimated ET from the different vegetation index products NDVI (Normalized Difference Vegetation Index) and EVI (Enhanced Vegetation Index) from MODIS.

2. MATERIALS AND METHODS

2.1 Study Area

2.1.1 Geographical extent

The Brahmaputra River basin within Indian and Bhutanese premises is chosen as the study area. The choice of study area was on the basis of presence fresh river basins which makes it a very important hydrological aspect of India. The geographical extent of study area lies between longitude 88.72–97.40 E, and latitude 25.08–29.47 N, with an elevation of 16–7467 m above the mean sea level. The total area of the study area is approximately 223185 km2. The study area is shown in Figure 1.

2.1.2 Basin and sub-basins

The Northern extents of the basin are covered by Arunachal Pradesh and Bhutan in proximity to the Eastern Himalayas. These areas contribute fresh water to Brahmaputra River from the tributaries developed from snow of from Eastern Himalayas. The central basin is mostly flood plains covered by Assam, originated at Arunachal Pradesh at the upstream end, and supported by some parts of West Bengal at the downstream end. The lower basin is covered by states of Nagaland at the upstream end, and Meghalaya at the downstream end. The contribution of these areas to Brahmaputra River is mostly by runoff resulted from precipitation from forests of Nagaland and Garo hills of Meghalaya.

2.1.3 Brahmaputra River system

The main stream of Brahmaputra river in the study basin is approximately 1036 km. After passing through the Great Bend in China, the main stream is referred to as Siang on entering to India. Flowing 35 km southwest through the Assam Valley, the river is joined at the start of valley by two other tributaries, Dibang and Lohit from Arunachal Pradesh to become the Brahmaputra. On its passage, the Brahmaputra is joined by tributaries, first by Subansiri, originated from Tibet, followed by Kameng originated from Tawang, Arunachal Pradesh. The tributaries described so far are the contributors of

Northern extents of the basin to main stream of Brahmaputra River. The southern basin adds fresh water from the tributaries Dhansiri from Laisang peak of Nagaland, followed by Kopili from Meghalaya, with the passage of main stream of Brahmaputra River towards Bangladesh. Though the main trunk of the Brahmaputra does not pass through Bhutan, the nation of Bhutan is entirely within the Brahmaputra watershed, and contributes water in four major tributaries: Amochu, Wang Chu, Sonkosh, and Manas, which finally joins the main stream of Brahmaputra River in Bangladesh to be called as Jamuna. The drainage map of the study area is presented in figure 1.

2.1.4 Climate

The study area is covered by five states in India (Arunachal Pradesh, Assam, Meghalaya, Nagaland, and West Bengal), Bhutan, and some parts of Bangladesh. The basin consists of three major ecological zones (Eastern Himalayas, Assam Bengal Plains, and Northeastern Hills). The map of ecological zones within the study area is shown in figure 1. The Eastern Himalayas ecological zone has a climatic variation with elevation. Areas at a very high elevation close to the Tibetan border have an alpine or tundra climate; middle regions have a temperate climate; lower regions generally experience humid, sub-tropical climate with hot summers and mild winters. The Assam Bengal Plains ecological zone experiences tropical monsoon rainforest climate, which is temperate and experiences heavy rainfall and high humidity. It is characterized by heavy monsoon downpours reducing summer temperatures (May–mid-June). The monsoon is experienced in the months of mid-June–August. Spring (March–April) and autumn (September–October) are usually moderate in rainfall and temperature. The Northeastern Hills ecological zone includes the Northern parts of the Meghalaya, and Northern Nagaland. The Meghalaya regions in the study area comprises of the Garo Hills region with lower elevations, which experiences high temperatures for most of the year. The Northern Nagaland in the study area enjoys a salubrious climate. Summer is the shortest season in the state that lasts for only a few months. Winter makes an early arrival and bitter cold and dry weather, and strong north-west winds are experienced across the regions during the months of February and March.

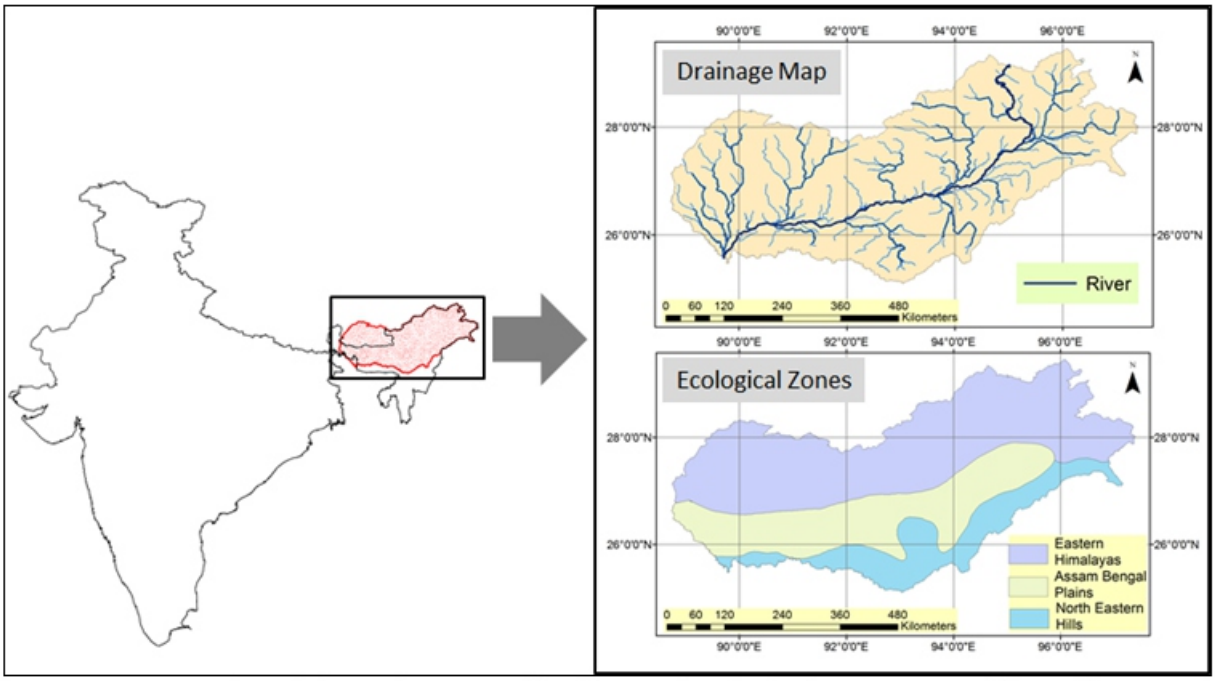

Figure 1 Location of the study area, and drainage and ecological zones maps of the study area

2.2 Methodology

2.2.1 Data and Preprocessing

There is a very large variation in climatic conditions and land features in the study area. It is influenced by variation in temperature, precipitation, humidity, forest type etc. in plain regions and mountainous regions. Thus, it is very difficult to estimate environmental parameters throughout such vast area. Remote sensing datasets could be useful in this case. The following study includes the remote sensing datasets as follows, 8-day land surface temperature/emissivity at 1-km (MOD11A2), 16-day Vegetation Index (NDVI, EVI) at 1-km (MOD13A2), and 16-day albedo at 1-km (MCD43B3) measured by MODIS Terra, obtained from the website of NASA's (EOSDIS) Earth Observing System Data and Information System (https://reverb.echo.nasa.gov/). MODIS/Terra + Aqua product (MCD12Q1) land cover data at 500 m spatial resolution was also obtained from EOSDIS. Time period of the study was fixed as the year of 2000 to 2010. All the datasets were brought to a common coordinate system by using the software ArcGIS. The land surface temperature 8 day composites at 1-km resolution were processed to generate 16 day composites to rhyme with 16 day scale. It was done by either averaging or allocation based on the incidence of land surface temperature per pixel. Air temperature for the study area was obtained as generated point from weather data provided by (CFSR) Climate Forecast System Reanalysis of (NCEP) National Centres for Environmental Prediction (https://rda.ucar.edu/)., which was again aggregated to match with the fixed 16 day scale. These points were interpolated using the krigging type interpolation using ArcGIS, to prepare distributed air temperature throughout the study

area. The SRTM (Shuttle Radar Topographic Mission Digital Elevation Model) DEM data at a spatial resolution of 90 m were downloaded from the website of Consortium for Spatial Information (http://cgiar-csi.org/), mosaicked and resampled at 1 km spatial resolution (Figure 2).

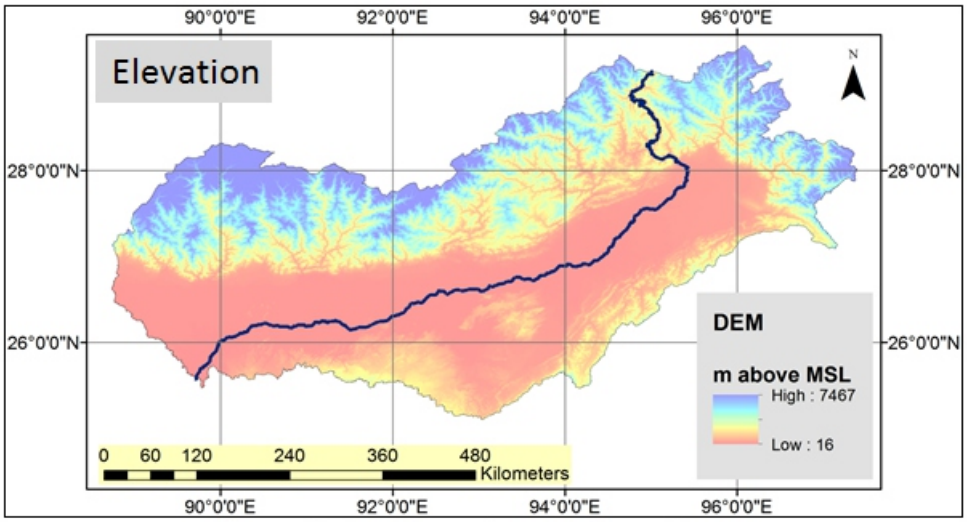

Figure 2 Elevation variation in the study area

2.2.2 Theory of 3T Model

The basic concept for 3T model is surface energy balance. It is assumed for this model that the land cover consists of three groups which are bare soil, vegetation and a mixture of both soil and vegetation. Algorithms have been established by Qiu et al. (1996) and Qiu et al. (1998) to calculate ET for areas having bare soil and vegetation respectively. Also algorithm to calculate ET for mixture of both soil and vegetation has been established by Xiong et al. (2008) using fractional vegetation cover which quantifies the presence of vegetation cover.

According to the general energy balance equation, energy exchange on earth surface can be express as:

$$LE = R_n - G - H \quad (1)$$

where L is the latent heat of vaporization with value 2.49×10^6 $W/(m^2 mm)$; LE is the latent heat flux; and E is the soil evaporation in mm; R_n is the net radiation at the soil surface; G is soil heat flux. Units of LE, R_n and G are in W/m^2. H is the sensible heat flux between land and atmosphere in W/m^2 which can be derived from the following equation as:

$$H = \frac{\rho C_P (T_s - T_a)}{r_a} \quad (2)$$

where ρ is the air density in kg/m^3, C_p is the specific heat at constant pressure in $MJ/(kg\ ^\circ C)$; T_s and T_a are soil surface temperature and air temperature respectively in $^\circ C$; r_a is the aerodynamic resistance in s/m, the diffusion resistance of the air layer.

In presence of a reference surface of dry soil with no significant modification in atmospheric conditions around it, the r_a of the dry soil and the r_a of the drying soil are approximately equal to each other; such conditions implies no water is in the dry soil and LE is negligible, hence the r_a can be evaluated by combining Eq. (1) and Eq. (2) (Qiu et al. 1999):

$$r_a = \frac{\rho C_P (T_{sd} - T_a)}{R_{n,d} - G_d} \quad (3)$$

where T_{sd} is the reference dry soil temperature, and $R_{n,d}$ and G_d are the net radiation and soil heat flux respectively for the reference dry soil. Thus, by combining Eq. (1), Eq. (2) and Eq. (3), soil evaporation (LE_s) can be estimated for pixels having pure soil as:

$$LE_s = R_{n,sm} - G - (R_{n,d} - G_d) \frac{(T_s - T_a)}{(T_{sd} - T_a)} \quad (4)$$

where T_s is the temperature and $R_{n,sm}$ is the net radiation of the soil. Similarly, by introduction of a canopy without transpiration (imitation canopy), r_a of the vegetation could be estimated using the formula:

$$r_a = \frac{\rho C_P (T_{cp} - T_a)}{R_{n,cp}} \quad (5)$$

where T_{cp} is the temperature and $R_{n,cp}$ is net radiation of the imitation canopy. Thus, by combining Eq. (1), Eq. (2) and Eq. (5), vegetation transpiration (LE_c) can be estimated for pixels having pure vegetation:

$$LE_c = R_{n,cm} - R_{n,cp} \frac{(T_c - T_a)}{(T_{cp} - T_a)} \quad (6)$$

where T_c is the temperature and $R_{n,cm}$ is the net radiation of the vegetation canopy.

Eq. (4) and (6) are the basic equations for computation of evaporation and transpiration and can only be used in case of pure pixels. The computation of evapotranspiration for the mixed region of soil and vegetation can be done by using fractional canopy coverage factor. Evapotranspiration in mixed pixels can be considered as:

$$LET = (1 - f)LE_s + fLE_c \quad (7)$$

where f is the fractional canopy coverage factor and can be calculated by the equation established by Carlson et al. (1995) as:

$$f = \frac{(VI - VI_{min})}{(VI_{max} - VI_{min})} \quad (8)$$

where VI is the Vegetation Index. Agam et al. (2007) have established the thresholds VI_{max} and VI_{min} selection method, in which these can be calculated from the lower and upper 3% tails of the VI distribution within the scene.

The dominance of a pixel going for only soil evaporation, only vegetation transpiration or evapotranspiration at a pixel depends upon category of the particular pixel. The category of pixels can be distinguished into pure or mixed pixel by using VI. Pixels with an VI larger than the VI_{max} are assumed to be pixel definitely containing pure vegetation cover; pixels with an VI less than the VI_{min} can be assumed to be covered by bare soil; pixels with a VI lying between VI_{min} and VI_{max} are assumed to be mixed pixels (Carlson et al. 1995).

In Eq.(1), R_n and G are the two parts which need to be estimated in order to compute LE. Eq.(1) is modified to Eq.(4) for soil and Eq.(6) for vegetation, out of which Eq.(4) requires estimation of R_n and G. Unlike Eq.(4), G is not required to be estimated in Eq.(6). However to compute Eq.(4) or Eq.(6), the land surface temperature needs to be separated for soil and vegetation. The entire procedure to calculate LE_s and LE_c can be listed as follows.

Net radiation

The net radiation (R_n) can be expressed as:

$$R_n = (R_{swd} - R_{swu}) + (R_{lwd} - R_{lwu}) \quad (9)$$

where R_{swd} and R_{swu} represents the incoming and outgoing shortwave radiation respectively; R_{lwd} and R_{lwu} represents the incoming and outgoing longwave radiation respectively. The shortwave radiation can be given by:

$$R_{swd} = \tau . S . E_0 . \cos\theta \quad (10)$$

$$\tau = 0.75 + 2 \times 10^{-5} \times h \quad (11)$$

$$E = 1 + 0.33 \cos\theta \ (2\pi DOY/365) \quad (12)$$

where τ is the atmospheric transmittance coefficient, which is a resultant of elevation (h) in m as in Eq. (11) (Allen et al. 1994); S is the solar constant (1367 W/m2); E is the eccentricity correction factor and can be calculated using day of the year (DOY), Eq. (12) (Allen et al. 1998); the number of the day in the year between 1 (1 January) and 365 or 366 (31 December); and θ is the solar zenith angle in terms of radian. Using the estimated R_{swd}, the net shortwave radiation can be calculated as:

$$R_{swd} - R_{swu} = (1 - \alpha) R_{swd} \quad (13)$$

$$\alpha = 0.160\alpha_1 + 0.291\alpha_2 + 0.243\alpha_3 + 0.116\alpha_4 + 0.112\alpha_5 + 0.081\alpha\_7 - 0.0015 \quad (14)$$

where α is the surface albedo that can be calculated as Eq. (14) (Liang 2001). $\alpha_1, \alpha_2, \alpha_3, \alpha_4, \alpha_5$ and α_7 are the reflectance of bands 1, 2, 3, 4, 5 and 7 respectively. The net longwave radiation can be expressed as:

$$R_{lwd} - R_{lwu} = \sigma\varepsilon_0\varepsilon_a(T_a + 273.15)^4 - \sigma\varepsilon_0 {T_s}^4 \quad (15)$$

$$\varepsilon_a = 9.2 \times 10^{-6} \times (T_a + 273.15)^2 \quad (16)$$

$$\begin{cases} \begin{cases} \varepsilon_0 = 0.9832 - 0.058\,\rho_1 \\ \Delta\varepsilon_0 = 0.0018 - 0.060\,\rho_1 \end{cases} & \text{VI} < 0.2 \\ \begin{cases} \varepsilon_0 = 0.9710 - 0.018\,\text{f} \\ \Delta\varepsilon_0 = -0.006(1-\text{f}) \end{cases} & 0.2 \le \text{VI} \le 0.5 \\ \begin{cases} \varepsilon_0 = 0.9900 \\ \Delta\varepsilon_0 = 0 \end{cases} & \text{VI} > 0.5 \end{cases} \quad (17)$$

where σ is the Stefan–Boltzmann constant with a value of (5.67×10^{-8} W/m^2); ε_a is the atmospheric emissivity and can be calculated from Eq. (16) (Swinbank 1963); ε_0 is the surface emissivity that can be calculated depending upon the NDVI value, Eq. (17) (Sobrino et al. 2004); and ρ_1 is the reflectivity acquired from band 1 (red band region) of MODIS.

The estimated R_n is the overall absorbed net radiation. For mixed pixels R_n needs to be separated in terms of net radiation absorbed by soil surface and vegetation canopy as:

$$R_{n,sm} = R_n \exp(-0.45\text{LAI}) \quad (18)$$

$$R_{n,cm} = R_n[1 - \exp(-0.45\text{LAI})] \quad (19)$$

$$\text{LAI} = -2\ln(1-\text{f}) \quad (20)$$

where R_n is the mixed net radiation absorbed by features in the pixel; $R_{n,sm}$ is the net radiation absorbed by soil surface; $R_{n,cm}$ is the net radiation absorbed by vegetation canopy; LAI is the leaf area index. The LAI can be derived from f as shown in Eq.(20) (Walthall et al. 2004). $R_{n,sm}$ and $R_{n,cm}$ can be further implemented in Eq.(4) and Eq.(6).

Net radiation for the reference surfaces i.e. reference dry soil ($R_{n,d}$) and imitation canopy ($R_{n,cp}$) can be expressed as:

$$R_{n,d} = (1-\alpha_{r,d})R_{swd} + \varepsilon_{0r,d}\varepsilon_a\sigma T_a^{\,4} - \sigma\varepsilon_{0r}T_s^{\,4} \quad (21)$$

$$R_{n,cp} = (1-\alpha_{r,cp})R_{swd} + \varepsilon_{0r,cp}\varepsilon_a\sigma T_a^{\,4} - \sigma\varepsilon_{0r}T_s^{\,4} \quad (22)$$

where empirical coefficients $\alpha_{r,d} = 0.275$ (Qiu et al. 1998); $\alpha_{r,cp} = 0.225$ (Qiu et al. 1996); $\varepsilon_{0r,d} = 0.970$ and $\varepsilon_{0r,cp} = 0.99$ (Sobrino et al. 2004). $R_{n,d}$ and $R_{n,cp}$ can be further implemented in Eq.(4) and Eq.(6).

Soil heat flux

The soil heat flux (G) can be estimated as per the established equation in the work by Su (2001):

$$G = R_n.[\Gamma_c + (1-\text{f}).(\Gamma_s - \Gamma_c)] \quad (23)$$

where the empirical coefficients $\Gamma_c = 0.05$ (Monteith 1973) and $\Gamma_s = 0.315$ (Kustas and Daughtry 1990). And the soil heat flux for reference dry soil (G_d) can be expressed as:

$$G_d = 0.315R_{n,d} \quad (24)$$

G and G_d can be further implemented in Eq.(4) to calculate soil evaporation (LE_s).

Land surface temperature separation

The estimation of LE_s and LE_c requires the separation of the land surface temperature which represents mixed temperature. The components of (T_s) are temperature of soil (T_{sm}) and vegetation (T_{cm}) to be implemented in Eq.(4) and Eq.(6) respectively. It can be separated by solving the following set of equations suggested by Lhomme et al. (1994), which are:

$$fT_{cm} + (1 - f)T_{sm} = T_s \quad (25)$$

$$T_{sm} - T_{cm} = a(T_s - T_a)^m \quad (26)$$

where T_s is the mixed land surface temperature; $a = 0.1$ and $m = 2$ are the empirical coefficients, (Lhomme et al. 1994). The temperature for reference dry soil (T_{sd}) for Eq.(4) and imitation canopy (T_{cp}) for Eq.(6), can be allocated as the maximum temperatures of soil and vegetation obtained respectively from Eq.(25) and Eq.(26) as proposed by Zhao et al. (2010).

Daily evapotranspiration

The algorithm described above estimates the ET, which is instantaneous. ET on a daily scale can be derived on the basis of derivation from instantaneous ET according to Jackson et al. (1983):

$$ET_d = \frac{ET_i . 2N_E}{\pi . \sin(\pi . t / N_E)} \quad (27)$$

where ET_d is the daily ET; ET_i is the instantaneous ET; N_E is the daily number of ET hours and is equal to the time interval between sunrise and sunset minus two; t is the time interval between sunrise and the data acquisition time i.e. time of satellite sensor pass.

2.2.3 Results and Discussion

The preprocessed datasets were used in 3T model to estimate instantaneous evaporation(LE_s), transpiration (LE_c), and evapotranspiration (LET), which were later converted to daily evaporation (E_s), transpiration(E_c), and evapotranspiration (ET). This was done for a period of years 2000-2013.The temporal variation of spatial average for the parameters E_s, E_c, and ET in the basin were calculated at 16 days intervals and analyzed for both EVI and NDVI as VI.

Spatial dynamics

The maps of the preprocessed datasets of day 321, year 2013, used as input for 3T model are shown in figure 3. The 3T model was used to estimate the spatial dynamics of the parameters E_s, E_c, and ET in (mm/day), by utilization of fractional vegetation cover prepared from both the vegetation index, NDVI and EVI. The EVI (Huete et al. 1994; Huete et al. 1997) has been found to perform better than NDVI at numerous occasions (Huete et al. 2002; Gurung et al. 2009; Feng et al. 2014). The reason is that NDVI exhibits scaling problems, saturated signals over high biomass conditions, and is very sensitive to canopy background variations with NDVI degradation particularly strong with higher canopy background brightness, whereas EVI was developed by de-coupling of the canopy background signal and a reduction in atmosphere influences (Huete et al. 1994; Huete et al. 1997). As far as the spatial variability is concerned, EVI products have the capability to provide detailed dynamics. A comparison between NDVI and EVI products by visual interpretation shows that fine details are well

exposed by EVI (figure 3). Similar visual interpretations in figure 4 show that the details exposed by outcomes from EVI are finer than that from NDVI.

Ranges

The fractional vegetation cover derived from different vegetation index products differ, which is crucial in defining the magnitude of outcomes. In figure 5, the temporal variation of spatial average for the parameters E_s, E_c, and ET in the basin at 16 days intervals are shown from years 2000–2013. The cyclic pattern of ET variations could be clearly seen in figure 5. It shows increase in magnitude of E_s, E_c, and ET from starting of the year, highest during monsoon, and then reducing again at the end of the year.

It is already a well-known fact that transpiration can never exceed evaporation in natural conditions (Herbst and Kappen 1999; Sutanto et al. 2012). The outcomes from NDVI shows frequent errors encountered, as the value of E_c exceeds E_s, marked by arrows in figure 5. These errors are generally encountered during the post–monsoon, when the magnitude of ET is highest in the year. The errors are caused due to insufficient availability of albedo and land surface temperature during monsoon season. The estimations in the spatial scene are restricted under empirical equations, but relative in nature within the scene, due to which the magnitude of E_c shows tremendous increase than its original value. With this increase in magnitude of E_c, ET value rises too. Estimations from both EVI and NDVI suffer from this problem; however the value of E_c form EVI was seen to exceed its E_s in only one case. It was also found that the overall Transpiration to Evaporation ratio was 22% and 48% in cases of EVI and NDVI respectively. It could be clearly seen in figure 5 that the gap between Transpiration and Evaporation is larger in EVI than in case of NDVI and maintained throughout the analyzed years. From this observation, it was interpreted that EVI is more reliable product to use than NDVI for ET estimations using 3T model. Therefore, the further estimations in the study was based on EVI as the vegetation index input.

Ecological zones

The study area is divided into three ecological zones. Table 1 shows the area covered by major features in the study area in various ecological regions. It was found that the largest proportion of area in Eastern Himalayas is covered by mixed forest, evergreen forest, and grasslands; cropland, natural vegetation, and savanna in Assam-Bengal Plains; and Evergreen forest, savanna, and mixed forest in Northeastern Hills. The land use and land cover map prepared for the study area obtained from MCD12Q1 MODIS product is shown in figure 6.

Table 1 Area covered by various classes in the study area in the ecological regions

Class	Area (km^2)	Eastern Himalayas	Assam- Bengal Plains		Northeastern Hills	
		Area (%)	Area (km^2)	Area (%)	Area (km^2)	Area (%)
Water	59	0.05	1587	2.47	91	0.24
Evergreen forest	39682	32.79	5452	8.48	21171	55.6
Deciduous forest	26	0.02	4	0.01	0	0
Mixed forest	52266	43.19	498	0.77	4276	11.23

Shrub land	522	0.43		1325	2.06	73	0.19
Savanna	3911	3.23		8687	13.51	9508	24.97
Grassland	15188	12.55		1699	2.64	127	0.33
Wetland	219	0.18		454	0.71	50	0.13
Cropland	1239	1.02		27520	42.8	1050	2.76
Urban area	41	0.03		311	0.48	58	0.15
Natural vegetation	4385	3.62		16122	25.07	1642	4.31
Snow and ice	3169	2.62		0	0	0	0
Barren land	317	0.26		639	0.99	32	0.08
Total Area	120805 km^2			64298 km^2		38079 km^2	

From the above observations it was decided to highlight only top three classes on the basis of area proportion in ecological zone. The average ET calculated for three largest classes in the ecological zones during 2000–2013 is represented in figure 7. The cyclic pattern is clearly visible in figure 7. The total ET is noticed to be at its peak during the post-monsoon and mid-monsoon. The Eastern Himalayas is dominated by evergreen and mixed type forests and a large proportion is covered by grasslands. The average annual ET of the forests in Eastern Himalayas is generally higher throughout the year, except for the post-monsoon and mid-monsoon, where the ET from the grasslands overcomes the total ET from forests. The mixed type forest is observed to have most ET throughout the ET cycle. Croplands are the most dominant class in Assam-Bengal Plains, still natural vegetation and savanna were found to have more ET than croplands. The savanna was noticed to show abnormal rise during post-monsoon and mid-monsoon.The hills of Northeastern Hills ecological zone have maximum area as forest cover. Evergreen forest and savanna were found to behave with evident rise during post-monsoon and mid-monsoon. The rest of the year, the general ET cycle is same for forests and savanna.

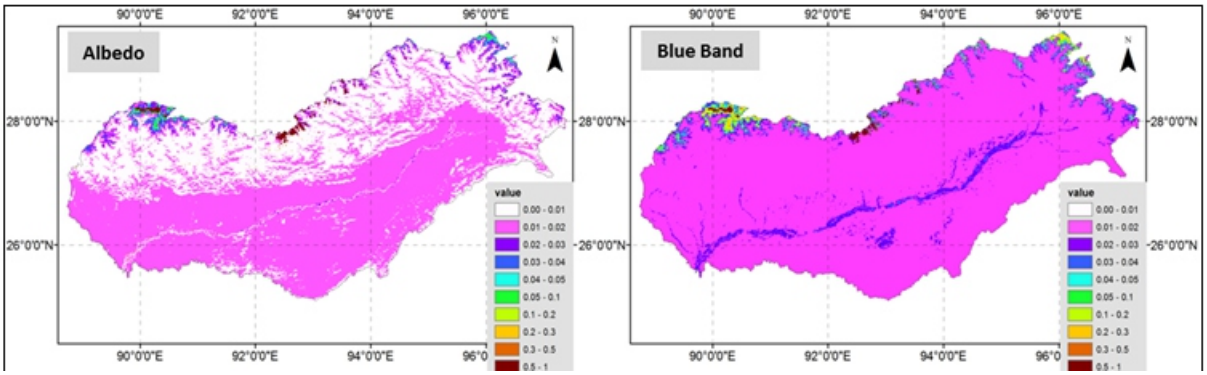

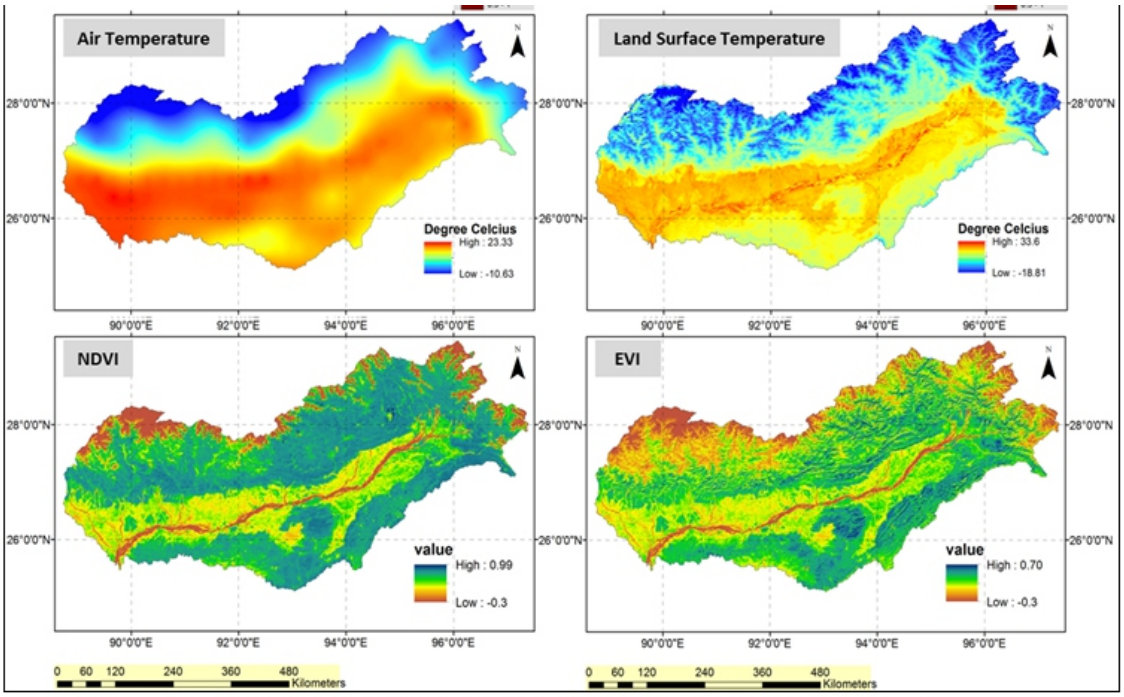

Figure 3 Preprocessed inputs for 3T model day 321-337, year 2013

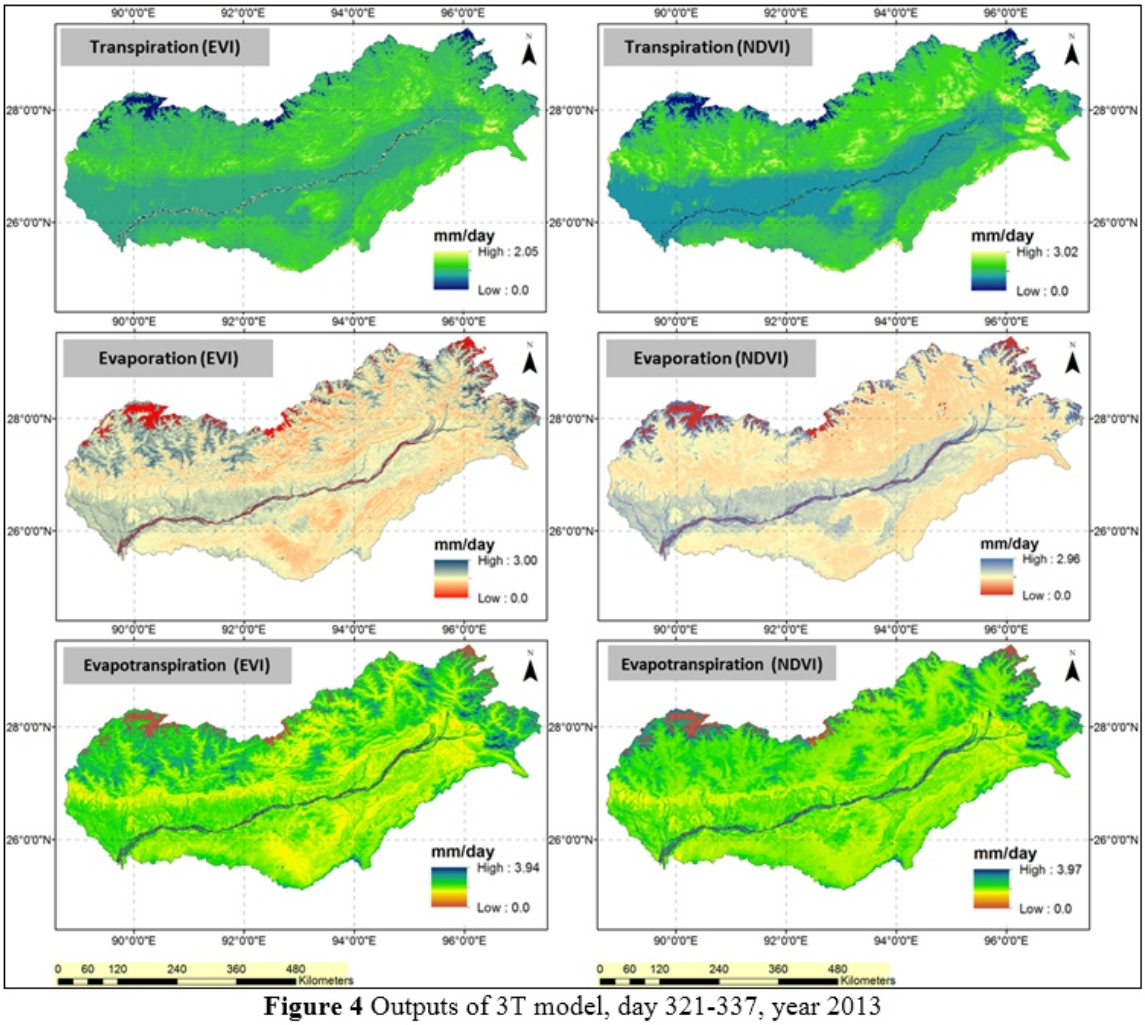

Figure 4 Outputs of 3T model, day 321-337, year 2013

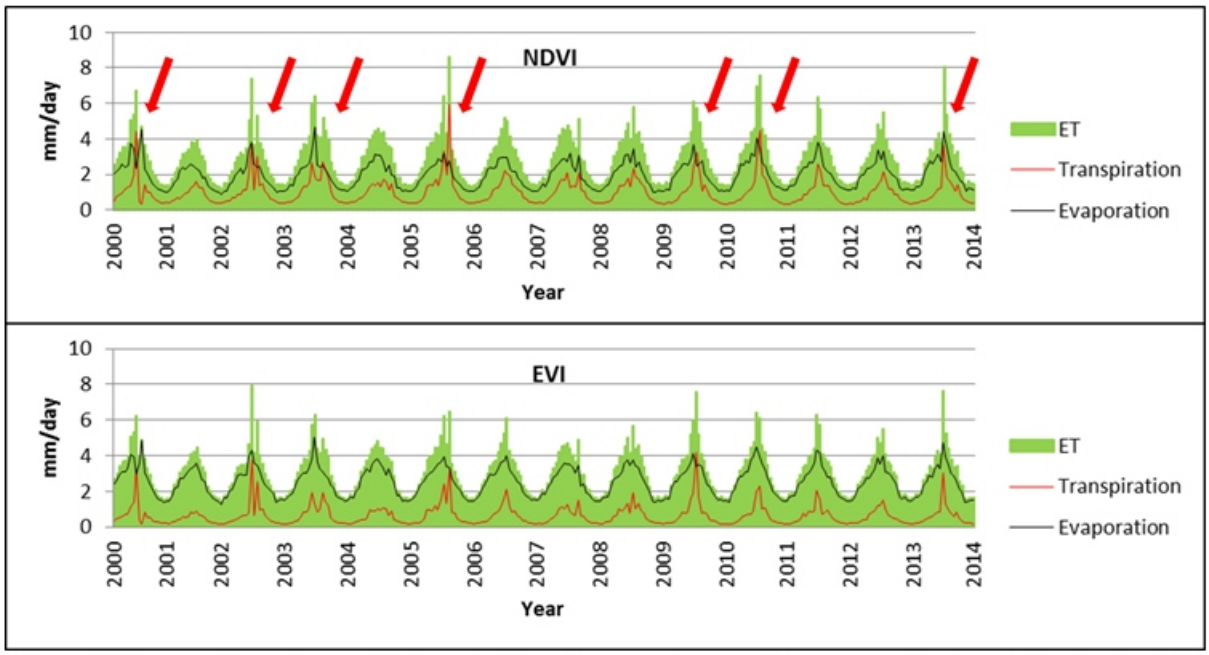

Figure 5 Temporal variations of Transpiration, Evaporation and Evapotranspiration in the basin at 16 days scale, years 2000–2013

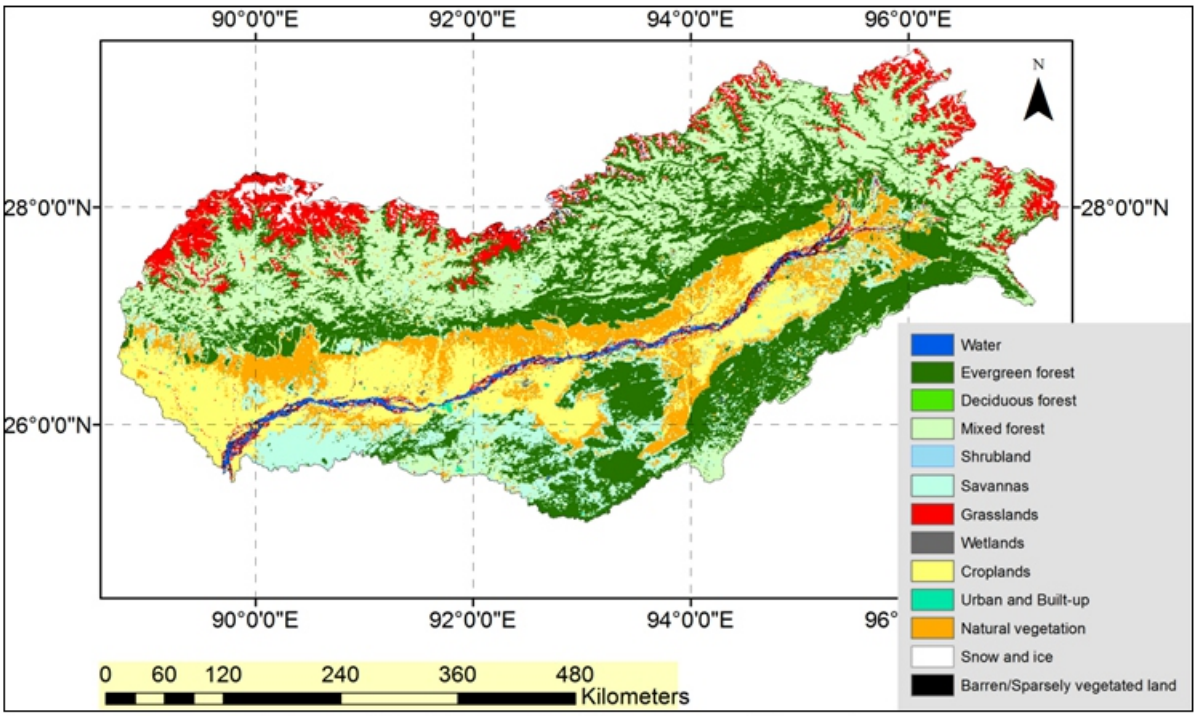

Figure 6 Land use and land cover map of the study area

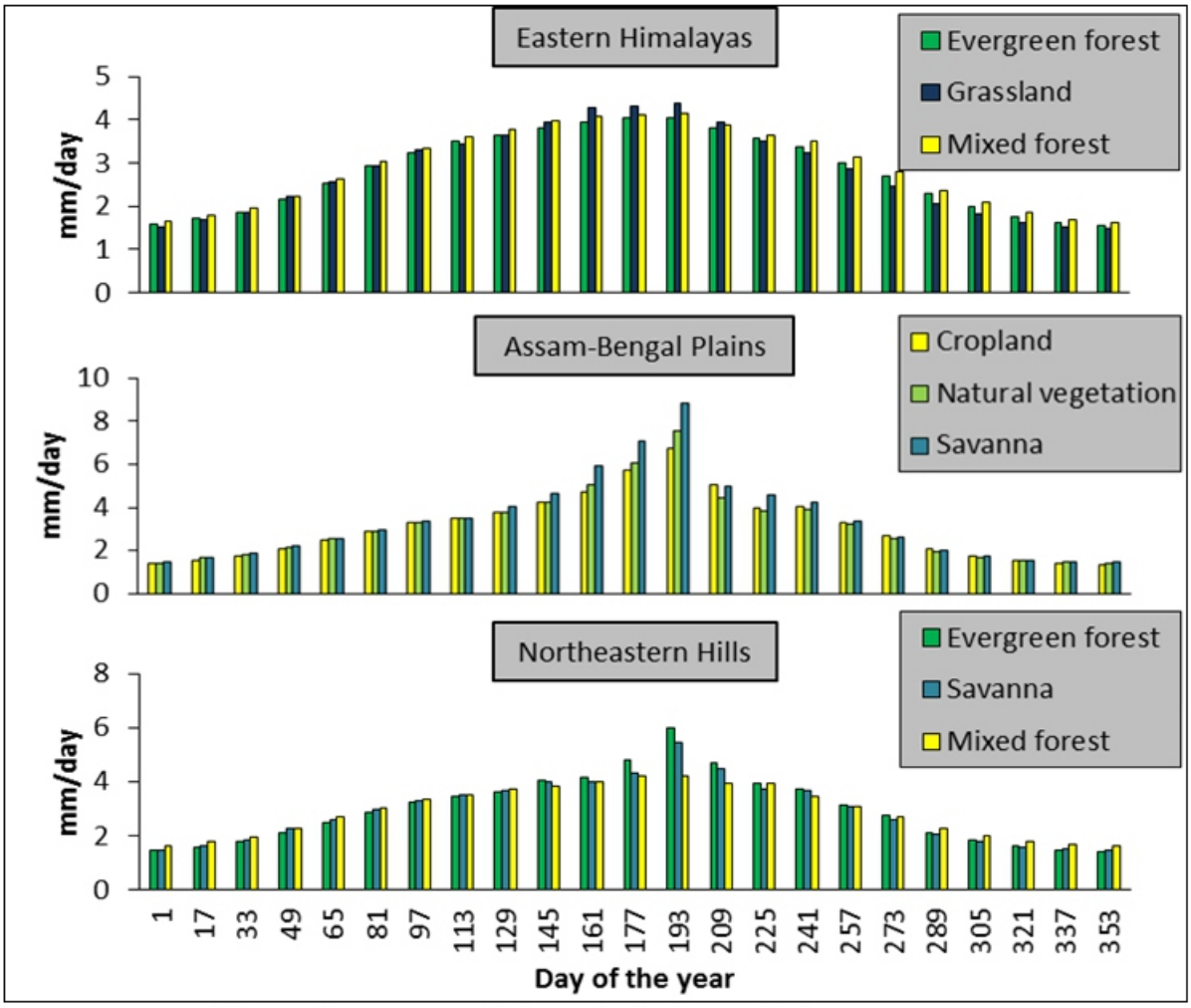

Figure 7 Average ET in the ecological zones during 2000–2013

3. CONCLUSIONS

The extended 3T model promises to be one of the simplest techniques of ET computation by using mostly remote sensing data and very few in-situ data. However, the extended 3T model has some drawbacks. Firstly, dynamics of ET distribution depends upon the albedo, which can have errors if cloud cover is present during image acquisition. Secondly, there lies the uncertainty in data itself which can cause errors. A ±10% change in LST will result in 34.17% and 82.48% change of ET estimations; 10% changes in R_n and G can result in an 8% and 5% change of ET (Sun et al. 2009). Thirdly, temperatures for reference dry soil surface and imitation vegetation are not appropriate. The difference in of these temperatures from actual ones can cumulate the error throughout the spatial coverage.

On the other hand extended 3T model have some advantages also, which proves to be reliable for remote locations, where partially or fully, measurement of ET is not possible. It also provides a good algorithm to compute soil evaporation and vegetation transpiration separately. This study provided

visions for ET estimation with qualitative information for the entire Arunachal Pradesh. This methodology has the potential for being useful to develop water budgets and to make informed decisions in concern to water resource management. The Transpiration to Evaporation ratio was found to be 22% and 48% in cases of EVI and NDVI. The performance of EVI is better than NDVI in estimation of ET and is preferable to be used in 3T model. It was found to be well distinctive for different land cover classes in different ecoregions.

REFERENCES

Agam, N., Kustas, W.P., Anderson, M.C., Li, F., and Neale, C.M.U. (2007). A vegetation index based technique for spatial sharpening of thermal imagery. Remote Sensing of Environment, 107, 545–558.

Allen, R.G., Pereira, L.S., Raes, D., and Smith, M. (1998). Crop evapotranspiration guidelines for computing crop water requirements. FAO irrigation and drainage paper, 56.

Allen, R.G., Smith, M., Pereira, L.S., and Perrier, A. (1994). An update for the calculation of reference evapotranspiration. ICID Bulletin, 43(2), 35–92.

Bastiaanssen, W.G.M., Menenti, M., Feddes, R.A., and Holtslag, A.A.M. (1998a). A remote sensing surface energy balance algorithm for land (SEBAL), Part 1, Formulation. Journal of Hydrology, 212–213, 198–212.

Bastiaanssen, W.G.M., Pelgrum, H., Wang, J., Ma, Y., Moreno, J.F., and Roerink, G.J. (1998b). A remote sensing surface energy balance algorithm for land (SEBAL), Part 2, Validation. Journal of Hydrology, 212–213, 213–229.

Carlson, T.N., Gillies, R.R., and Schmugge, T.J. (1995). An interpretation of methodologies for indirect measurement of soil water content. Agricultural and Forest Meteorology, 77, 191–205.

Gowda, P.H,, Chavez, J.L., Colaizzi, P.D., Evett, S.R., Howell, T.A., and Tolk, J.A. (2008). ET mapping for agricultural water management: present status and challenges. Irrigation Science, 26, 223–237.

Gurung, R.B., Breidt, F.J., Dutin, A., and Ogle, S.M. (2009). Predicting Enhanced Vegetation Index (EVI) curves for ecosystem modeling applications. Remote Sensing of Environment, 113, 2186–2193.

Herbst, M, and Kappen, L 1999, 'The ratio of transpiration vs. evaporation in a reed belt as influenced by weather conditions. Aquatic Botany, 63, 113-125.

Huete, A. R., Liu, H. Q., Batchily, K., and Van Leeuwen, W. J. D. (1997). A comparison of vegetation indices over a global set of TM images for EOS-MODIS. Remote Sensing of Environment, 59, 440 – 451.

Huete, A., Didan, K., Miura, T., Rodriguez, E.P., Gao, X., and Ferreira., L.G.(2002). Overview of the radiometric and biophysical performance of the MODIS vegetation indices. Remote Sensing of Environment, 83, 195–213.

Huete, A., Justice, C., and Liu, H. (1994). Development of vegetation and soil indices for MODIS-EOS. Remote Sensing of Environment, 49, 224 – 234.

Jackson, R.D., Hatfield, J.L., Reginato, R.J., Idso, S.B., and Pinter, P.J., (1983). Estimation of daily evapotranspiration from one time-of-day measurements. Agricultural Water Management, 7, 351–362.

Jiang, X.H., Liu, and C.M. (2010). The influence of water regulation on vegetation in the lower Heihe River. Journal of Geographical Sciences, 20(5),701–711.

Kite, G., and Droogers, P. (2000). Comparing evapotranspiration estimates from satellites, hydrological models and field data. Journal of Hydrology, 229, 3–18.

Kustas, W.P., and Daughtry, C.S.T. (1990). Estimation of the soil heat flux/net radiation ratio from spectral data. Agricultural and Forest Meteorology, 49(3), 205–223.

Lhomme, J.P., Monteny, B., and Amadou, M. (1994). Estimating sensible heat flux from radiometric temperature over sparse millet. Agricultural and Forest Meteorology, 68, 77–91.

Li, F., Kustas, W.P., Prueger, J.H., Neale, C.M.U., and Jackson, J.J. (2005). Utility of remote sensing based two-source energy balance model under low and high vegetation cover conditions. Journal of Hydrometeorology, 6, 878–891.

Liang, S.L. (2001). Narrowband to broadband conversions of land surface albedo I: algorithms. Remote Sensing of Environment, 76, 213–238.

Liu, J., Zehnder, A.J.B., and Yang, H. (2009). Global consumptive water use for crop production: the importance of green water and virtual water. Water Resources Research, 45, W05428.
Monteith, J.L. (1973). Principles of Environmental Physics, second ed. Edward Arnold Press, London, 241.
Mu, Q., Heinsch, F.A., Zhao, M., and Running, S.W. (2007). Development of a global evapotranspiration algorithm based on MODIS and global meteorology data. Remote Sensing of Environment, 111, 519–536.
Nemani, R., White, M., Thornton, P., Nishida, K., Reddy, S., Jenkins, J., and Running, S. (2002). Recent trends in hydrologic balance have enhanced the terrestrial carbon sink in the United States. Geophysical Research Letters, 29(10), 1468.
Qiu, G.Y., Momii, K., and Yano, T. (1998). An improved methodology to measure evaporation from bare soil based on comparison of surface temperature with a dry soil. Journal of Hydrology, 210, 93–105.
Qiu, G.Y., Momii, K., Yano, T., and Lascano, R.J. (1999). Experiment verification of a mechanistic model to partition evaporation into soil water and plant evaporation. Agriculture for Meteorology, 93, 79–93.
Qiu, G.Y., Yano, T., and Momii, K. (1996). Estimation of plant transpiration by imitation leaf temperature. Theoretical consideration and field verification. Transactions of the Japanese society of irrigation. Drainage and Reclamation Engineering, 64, 401–410.
Rosenberg, N.J., Blad, B.L., and Verma, S.B. (1983). Microclimate: The Biological Environment of Plants, second ed. John Wiley Sons, New York, 495.
Sobrino, J.A., Jiménez-Munoz, J.C., and Paolini, L. (2004). Land surface temperature retrieval from LANDSAT TM 5. Remote Sensing of Environment, 90(4), 434–440.
Su, Z. (2001). The surface energy balance system (SEBS) for estimation of turbulent heat fluxes. Hydrology and Earth System Sciences, 6(1), 85–99.
Sun, Z.G., Wang, Q.X., Matsushita, B., Fukushima, T., Ouyang, Z., and Watanabe, M. (2009). Development of a simple remote sensing evapotranspiration model (SimReSET): algorithm and model test. Journal of Hydrology, 376, 476–485.
Sutanto, S. J., Wenninger, J., Coenders-Gerrits, A. M. J., and Uhlenbrook, S. (2012). Partitioning of evaporation into transpiration, soil evaporation and interception: a comparison between isotope measurements and a HYDRUS-1D model. Hydrology and Earth System Sciences, 16, 2605–2616.
Swinbank, W.C. (1963). Long-wave radiation from clear skies. Quarterly Journal of the Royal Meteorological Society, 89(381), 339–348.
Tian, F., Qiu, G.Y., Yang, Y.H., Lu, Y.H., and Xiong, Y. (2013). Estimation of evapotranspiration and its partion based on an extended three-temperature model and MODIS products. Journal of Hydrology, 498, 210-220.
Walthall, C., Dulaney, W., Anderson, M., Norman, J., Fang, H.L., and Liang, S.L. (2004). A comparison of empirical and neural network approaches for estimating corn and soybean leaf area index from landsat ETM+ imagery. Remote Sensing of Environment, 92(4), 465–474.
Xiong, Y.J., and Qiu, G.Y. (2011). Estimation of evapotranspiration using remotely sensed land surface temperature and the revised three-temperature model. International Journal of Remote Sensing, 32(20), 5853–5874.
Zhang, F., Zhang, L.W., Shi J.J., and Huang. J.F. (2014). Soil Moisture Monitoring Based on Land Surface TemperatureVegetation Index Space Derived from MODIS Data. Pedosphere 24(4), 450–460.
Zhao, S.H., Yang, Y.H., Qiu, G.Y., Qin, Q.M., Yao, Y.J., Xiong, Y.J., and Li, C.Q. (2010). Remote detection of bare soil moisture using a surface-temperature-based soil evaporation transfer coefficient. International Journal of Applied Earth Observation and Geoinformation, 12, 351–358.

Analysis of Spatial and Temporal Variations of Urban Heat Island Effect on Ahmedabad city and its Relationship with Impervious Surfaces

Aneesh Mathew[1], Sumit Khandelwal[2], Nivedita Kaul[3]
[1]Research Scholar, Department of Civil Engineering, Malaviya National Institute of Technology Jaipur, Jaipur, 302017, India
[2,3]Assistant Professor, Department of Civil Engineering, Malaviya National Institute of Technology Jaipur, Jaipur, 302017, India
Email: aneesh52006@gmail.com
Mobile No.: +91 8502932688

ABSTRACT

Ahmedabad is one of the fastest growing metropolitan cities in India showing rapidly urbanizing agglomeration. Due to the rapid urbanization natural land surfaces are being replaced by the anthropogenic materials which negatively impacts the environment resulting in urban heat island (UHI) effect. Land surface temperature (LST) is the primary and key step for the analysis of UHI effect. The present study has been carried out to analyze the variations in rise in land surface temperatures in the urban area than the surrounding rural area for three different seasons' winter, summer and monsoon of the years from 2009 to 2013 using Moderate-Resolution Imaging Spectroradiometer (MODIS) sensor data. Analysis of 8-day night time LST data show that significant surface urban heat island (SUHI) exists over the Ahmedabad study area. UHI intensity over the study area varies with seasons. Average annual UHI intensity from 2009 to 2013 varies from 6.01 K to 6.56 K and overall average UHI intensity is 6.17 K. UHIindex has been used for the present study to compare the UHI intensity of different periods and different seasons. The average value of UHIindex for the study period has been calculated for all the pixels of the study area and maximum of average UHIindex is 0.94. Pixels with average value of UHIindex more than 0.9 have been considered to indicate that high LST normally occurs on these pixels and they have been considered as hot spots (HS). The relationship between LST and Percent impervious surface area (%ISA) has also been investigated in the present study. %ISA has been reported to be a good parameter for the analysis of UHI effect and its relationship with LST has also been reported to be season independent. The relationship between %ISA and LST is similar for all three seasons with a consistent rising trend..

Keywords—Urban Heat Island, Land Surface Temperature, MODIS, UHIindex, %ISA

1. INTRODUCTION

Global temperature is gradually and continuously rising in all cities of world. One of the main causes for this rise in temperature is urbanization, which in turn results in large scale deforestation. This creates enormous impacts on the environment at the local, regional and global scales. Urban heat island (UHI) is the phenomenon of significant rise of atmospheric and surface temperatures in urban areas when compared to the surrounding semi-urban and rural areas, mainly caused due to urbanization (Voogt & Oke, 2003). It is characterized by a large expanse of non-evaporating impervious materials covering a majority of urban areas resulting in an increase in sensible heat flux at the expanse of latent heat flux (Oke, 1982; Owen et al., 1998). LST is of prime importance to the study of urban climate and it is not only useful in obtaining boundary conditions of the atmosphere, but also in understanding the

environmental conditions necessary for human beings (Tran et al., 2006). Many studies have estimated the relative warmth of cities by using the air temperature measurements. For example, Karl et al. (1988) indicate that throughout the last century urbanization has created, for the annual mean temperature, a warm bias of 0.06 K in the climate record of the US. In a study of UHIs throughout China, an average increase of 0.1 K per decade, in the UHIs, has been observed since 1970s (Weng et al., 1990). It has also been found that UHIs have seasonal dependence which varies considerably across the country. Zhang et al (2010) have demonstrated remarkable increase of UHI intensity in Shanghai over the past three decades and rate of increase of 0.75 K per decade in the mean temperature has been observed. The temperature gradient has been observed to be from rural to suburban to urban area. They have found that, as a consequence of prevailing weather conditions, the UHI is strongest in autumn and weakest in the summer. Yuan & Bauer (2007) have investigated the relationship of LST with %ISA and have concluded that %ISA is an accurate indicator of SUHI effects with strong linear relationship between LST and %ISA for all study seasons. Zhang et al. (2009), utilizing data from TM and ETM+ imageries, have indicated strong positive correlation between %ISA, normalized difference built-up index (NDBI) and LST whereas the correlations between NDVI and LST have been found to be weak. The study suggests that %ISA combined with LST and NDBI can quantitatively describe the spatial distribution and temporal variation of urban thermal patterns and associated land-use/ land-cover conditions. Mathew et al. (2015) investigated that positive correlation exists between LST and NDBI in Ahmedabad city which means that built-up areas can strengthen the effect of UHI.

2. STUDY AREA

Ahmedabad, located on the bank of Sabarmati river, is the fifth largest city of India and former capital of Indian state Gujarat. Climatic condition of the Ahmedabad is semi-arid and hot because of less rainfall during monsoon season and the climate of the Ahmedabad is extreme hot from March to mid-June. Wind which blows from the north side provides cold chill during the month of January and monsoon brings humid climate in the month of mid-June to mid-September. Ahmedabad is situated on dry and sandy soil which absorbs more heat during day time which is released during the night, thereby making the environment of the city hotter than its surrounding rural areas creating environmental impact by temperature gradient called UHI effect of the city.

The urban area boundary of Ahmedabad city has been developed by extracting urban area polygon from the MODIS yearly land cover type image (MCD12Q1) of 2011 using raster to polygon conversion tool in ArcGIS. The length and width of urban area polygon is approximately 12 km in North-South direction and 17 km in East-West direction.

A buffer of 5 km has been created around the urban boundary and the study has been carried out for area falling within this boundary. In addition to urban areas, study area sufficiently includes rural/sub-urban

areas and satellite towns of the city. The study area covers approximately 745 square kms. The raster pixel size of LST product is 926.626 m and LST image of the study area has 804 pixels. Figure 1 shows the study area of Ahmedabad city.

Figure 1 Ahmedabad study area

3. DATA AND METHODOLOGY

Eight day, 1 km MYD11A2 land surface temperature and emissivity product of MODIS Aqua of overlapping dates and Landsat data have been used for the present study. The land surface temperature and emissivity product is available with quality flag which was checked to include only those pixels which satisfy good quality criteria in the analysis. Landsat Operational Land Imager (OLI) and Thematic Mapper (TM) sensor images have also been selected for the present study for their good imaging quality.

Table 1 Remote sensing data used for the present work

Remote Sensing Product	Short Name	Sensor	Platform	Temporal Resolution	Spatial Resolution (m)
Land Cover Type	MCD12Q1	MODIS	Combined Aqua & Terra	Yearly	463.3
Land Surface Temperature and Emissivity	MYD11A2	MODIS	Aqua	8 Day	926.6
Landsat	-	TM/OLI	-	-	30

Geometric rectification of Landsat images have been done to the UTM projection system (datum WGS 84, Zone 43N). The pixel values of the TM images have been converted to the ex-atmospheric reflectance using the methods provided by Chander and Markham and the Landsat 7 Science Data Users Hand book.

The downloaded MODIS data is in Sinusoidal Projection System and in HDF-EOS format. The Earth gridded tile area of each MODIS image covers approximately 1100 km x 1100 km. MODIS Re-projection Tools (MRT) have been used for the pre-processing of downloaded MODIS images. Sub setting of the data to smaller area has been done using MRT. MODIS data has also simultaneously been re-projected from Sinusoidal projection to the UTM projection system (datum WGS 84, Zone 43N) and has been reformatted from HDF-EOS to GeoTIFF format.

Linear spectral mixture analysis (LSMA) has been used in the present study for the extraction of impervious surfaces using ENVI 5.1 software. Landsat derived %ISA layers is approximately at 30 m ground resolution, whereas MYD11A2 product for Night LST has a resolution of approximately 926.6 m. In order to compare %ISA with LST, it is necessary to have both of them have same resolution so that %ISA layers were aggregated to the same resolution as of LST layer and they were also snapped to LST image.

4. RESULTS AND DISCUSSIONS

.1 LST pattern and UHI intensity of Ahmedabad city

LST analysis of Ahmedabad city has been done for five years (2009-2013) on season basis. The entire year is divided into winter, monsoon and summer season and the LST and UHI analysis have been done seasonally. LST images of the Ahmedabad city on the basis of different seasons are shown in figure 2. LST of urban area is higher as compared to the area outside the urban boundary and most of the pixels representing high temperature are within the urban boundary. Red colour in figure 2 which indicates higher temperature in central part of the city, and light bluish colour shows low temperature at periphery of the study area which come under rural belt, the temperature is low in rural areas because of green vegetation. Urban areas show higher temperature pixels due to the presence of impervious surfaces and anthropogenic materials in the urban areas compared to rural areas. The pattern of LST over the entire study area does not change significantly throughout the year.

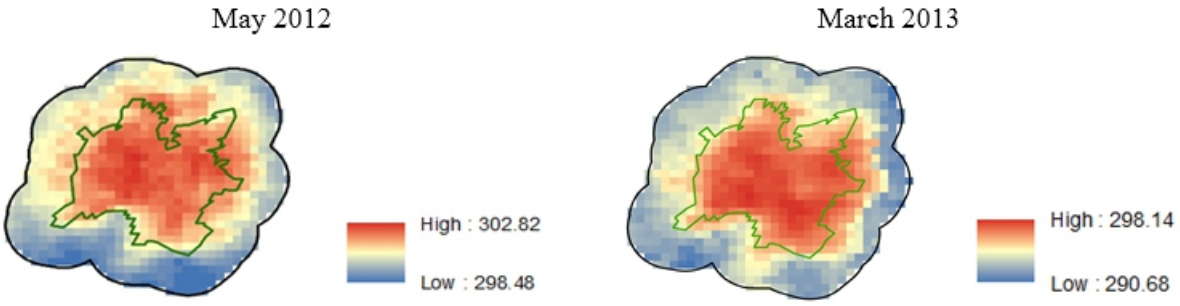

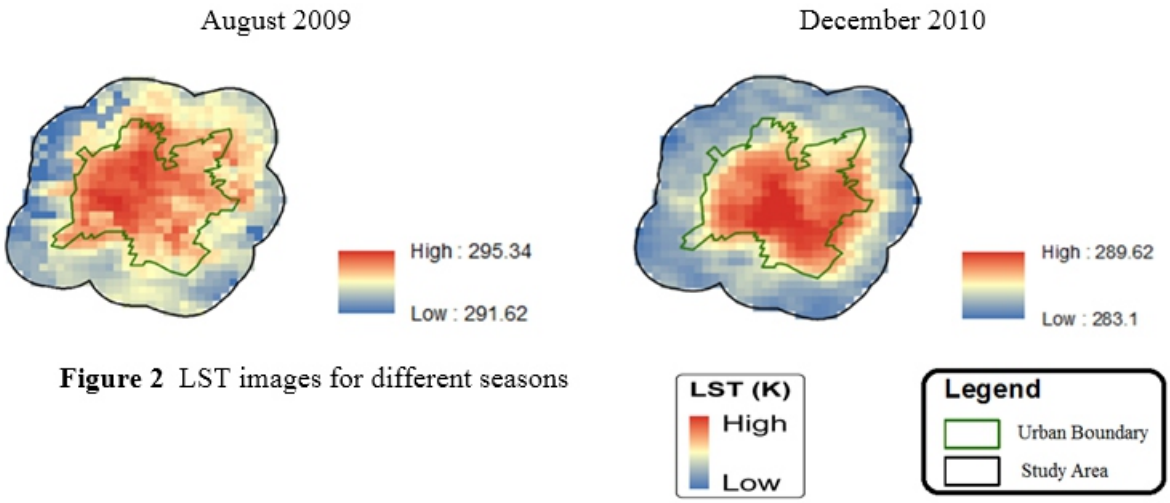

Figure 2 LST images for different seasons

Table 2 Average UHI intensity (K) during different seasons

Season	2009	2010	2011	2012	2013	Overall Average
Summer	5.955	6.228	6.088	5.916	6.127	6.063
Monsoon	4.678	5.387	6.533	5.022	5.287	5.381
Winter	7.398	6.754	7.065	7.155	6.978	7.070
Annual	6.010	6.123	6.562	6.031	6.130	6.171

Absolute maximum LST for summer season is found to be 304.2K and the absolute maximum LST values for winter and monsoon season are 298.78K and 301.38K respectively. Similarly absolute minimum values of LST for summer, monsoon and winter season are 285.46K, 285.42K, and 281.26K respectively.

UHI intensity exhibits diurnal and seasonal variations and is affected by meteorological conditions, such as cloud, wind conditions as well as anthropogenic heat release. Overall maximum UHI intensity has been recorded as 11.22k during monsoon season of 2011. The maximum UHI intensity of the study area during different seasons varies from 5.20K to 11.22K. Similarly minimum UHI intensity during different seasons varies from 2.22K to 6.56K. The maximum UHI intensity varies from 8.32 to 8.78K during summer season and 7.48 to 11.22K during monsoon season and 8.72 to 10.02K during winter season. Similarly minimum UHI intensity varies from 2.46 to 3.28K, 2.22 to 4.04K, 4.22to 6.56K for summer, monsoon and winter season respectively. It has been found out that raining during monsoon season increases the moisture content in the soil so that it absorbs more heat during day time and temperature of that kind of environment will increase so that sometime LST is more during monsoon season in the rural area or villages around the Ahmedabad city. Average UHI intensity of different seasons varies from 4.68K to 7.39K. Overall average UHI intensity of the study area during monsoon,

season in the rural area or villages around the Ahmedabad city. Average UHI intensity of different seasons varies from 4.68K to 7.39K. Overall average UHI intensity of the study area during monsoon, summer and winter seasons is 5.38K, 6.06K, and 7.07K respectively. Overall average SUHI intensity of the study area for all seasons is 6.17K.

The maximum and minimum temperatures for different periods of different years are highly variable, depending on the season of the year. Similarly, the UHI intensity at a particular area also varies considerably. Due to these reasons, it is very difficult to compare UHI intensity at a particular location or UHI intensity of different locations during different periods. Further, it is not possible to calculate the consolidated UHI effect over the study area from the LST data of a long period. In order to facilitate such calculations, LST values of all pixels of an image have been normalized between 0 and 1, using UHIindex. UHIindex has been calculated as

$$UHI_{index}=(LST_i - LST_{min})/(LST_{max} - LST_{min}) \quad (1)$$

Where LST_i is the LST of the pixel for a particular image, LST_{max} is the maximum value of LST, LST_{min} is the minimum value of LST of the same image as that of the LST_i.

UHIindex of all the pixels of the study area has been calculated for the entire study period (193 images of 5 years from 2009 to 2013) and average of the UHIindex of all the images has been calculated. Figure 3 shows the average normalized UHI intensity (UHIindex) over the study area. Maximum value of average UHIindex is 0.94 and all the four pixels in red colour in figure 3 correspond to average UHIindex value of more than 0.90. These pixels which are the part of the CBD of Ahmedabad city are the centre of the heat island. Other high temperature pixels are located around these pixels.

The urban area has only high temperature pixels and the minimum value of average UHIindex in the urban area is 0.328 and mean of average UHIindex of the urban area is 0.732. Similarly, the maximum and minimum values of average UHIindex corresponding of rural area are 0.827 and 0.181, respectively. Minimum average UHIindex value of 0.181 indicates that minimum temperature pixels of the entire study area are not same during different periods. Mean of average UHIindex corresponding to rural area is 0.352.

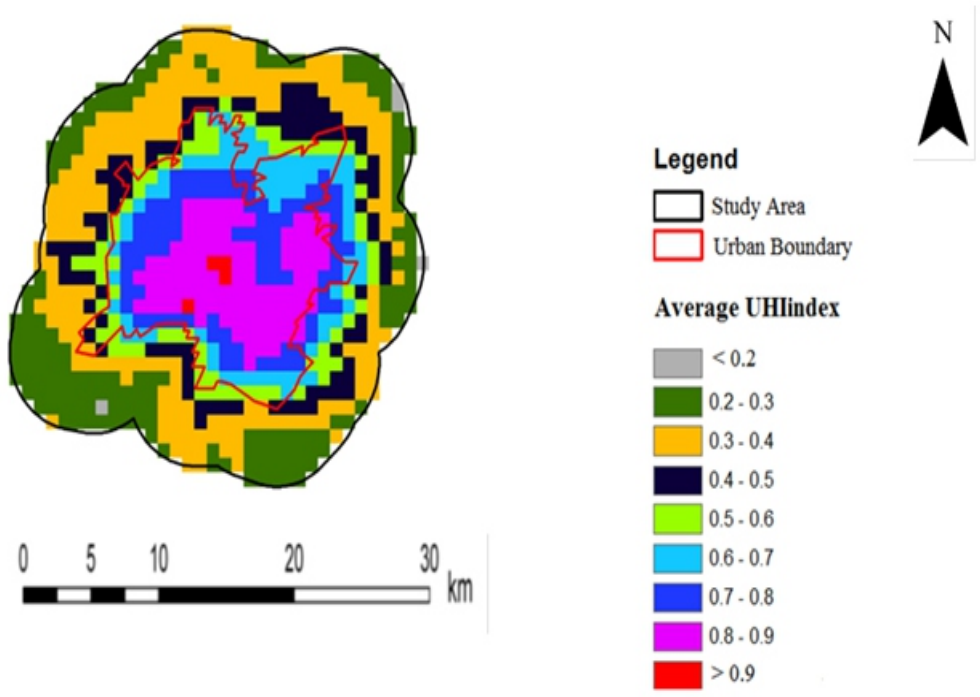

Figure 3 Average UHI_{index} image of the study area

The overall temperature pattern is similar to that discussed earlier and the UHIindex can be conveniently used for comparison of UHI intensity at a particular location during different periods or UHI intensity of different locations during different periods

4.2 Pattern of percent impervious surface area (%ISA)

Percent Impervious Surface Area has emerged as a key factor to explain and generally predict the degree of impact severity on Land surface temperature. Imperviousness provides an objective measurement of the areal extent and intensity of urban development. The resulting classification provides a continuous range of impervious area from 0 to 100%. In the present study, it has been observed that in all three seasons the pattern of impervious surfaces is almost same in the study area. %ISA is season independent. In order to analyse the spatial pattern of impervious surfaces of the study area, %ISA images for different periods of the study area are shown in figure 4.

Urban areas show higher values of %ISA compared to rural areas due to the presence of impervious surfaces like buildings, roads, parking lots etc. Agricultural land and vegetated areas in rural areas show zero %ISA. Bare soil in rural areas show very low values of %ISA compared to urban areas.

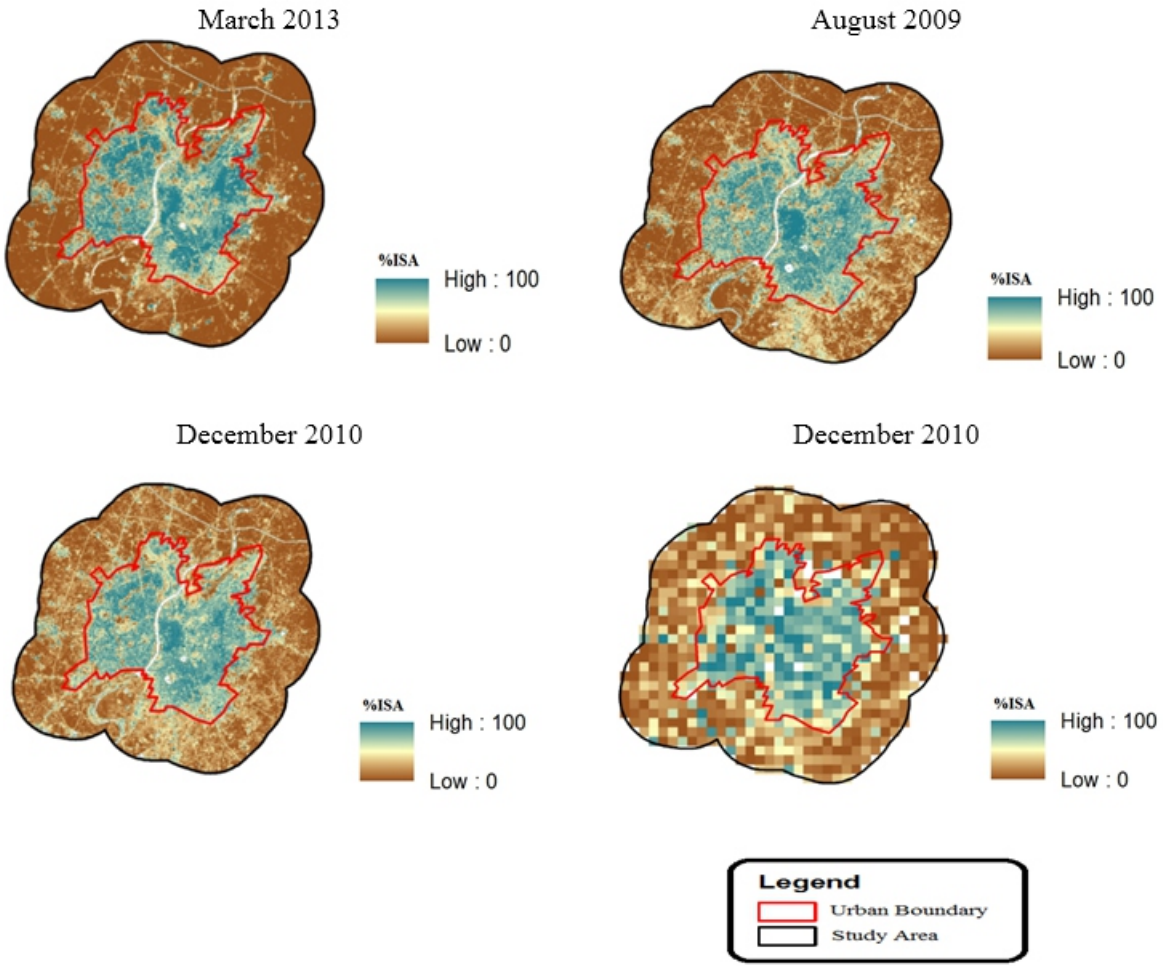

Figure 4 Landsat %ISA images of the study area for different seasons

The values of %ISA have been calculated at the Landsat TM/OLI resolution of 30m and at the aggregated resolution of 926.6 m. The overall absolute maximum and minimum %ISA values of the study area are 0 and 100 respectively. The overall average of the %ISA of the study area varies from 25.26% to 36.92%. Figure 4 shows the original %ISA image (at 30m resolution) and aggregated %ISA image (at 926.6 m resolution).

4.2 LST relationship with %ISA

The scatter plots regarding LST-%ISA relationship for different years are shown in figure 5. The relationship between %ISA and LST is similar for all three seasons with a consistent rising trend. Though high variation can be observed in the scatter plots showing weak trend for low %ISA values but the trend is strong for high %ISA values. Normally %ISA values are very less in rural areas compared

to urban areas due to the lack of impervious surfaces like roads, built-up areas etc. which results in weak trend and also the presence of bare land, vegetation and agricultural field show very low %ISA values in rural areas which result in low surface temperature. The weak trend may be due to the fact that for low %ISA values, urbanization does not have a significant effect and hence LST variations are governed by combined effect of several other parameters such as vegetation cover and its disposition, type and extent of surface imperviousness, condition of nearby pixels etc. The improved trend for higher %ISA values indicates that for urbanized area, %ISA, compared to other parameters, has more effect on LST. Similar trend for different seasons indicate that unlike vegetation indices the relationship of %ISA with LST is independent of season. Impervious surface areas mainly account for surface urban heat island (SUHI) in the Ahmedabad study area due to the variations in land surface temperatures.

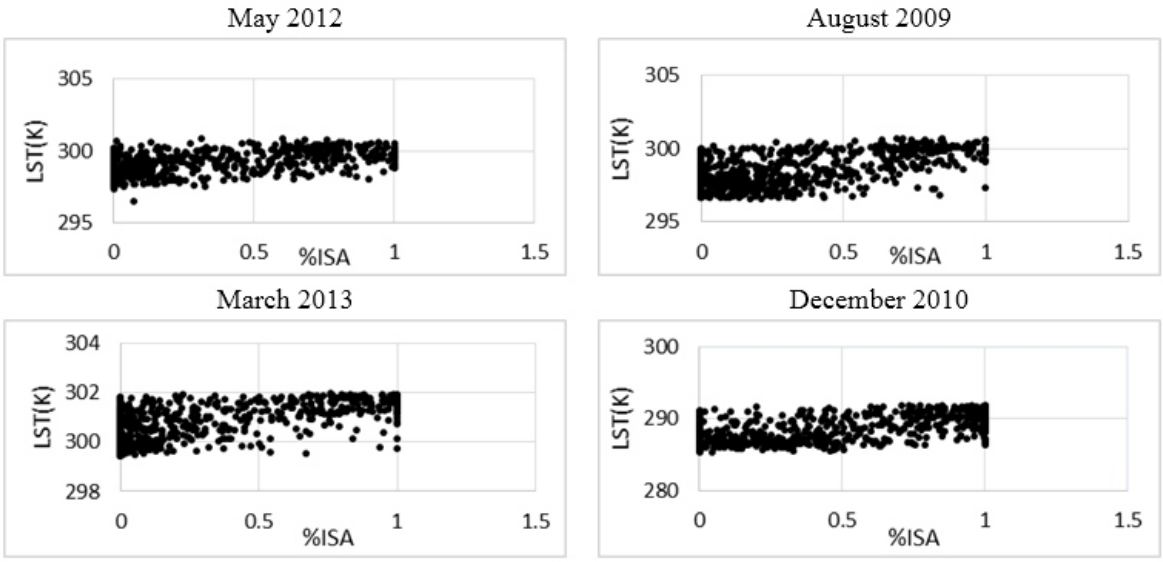

Figure 5 LST and %ISA scatterplots for different seasons

In the area of urban climate, Yuan and Bauer (2007) have documented a strong relationship between amount of impervious surface area and land surface temperatures or the urban heat island effect which is also validated from present study. Vegetation is also dependent on the extent of urbanization and it normally decreases with increase in urbanization. %ISA provides an objective measurement of the areal extent and intensity of urban development. %ISA is an indicator of urbanization which increases with growth of the city. It also takes into account, to some extent, the effect of anthropogenic heat produced due to various activities taking place in urban areas such as industries, heat due to air-conditioning, vehicular traffic etc. Hence analysis of SUHI effect using %ISA not only considers the impervious surfaces but it also accommodates, to some extent, the effect of anthropogenic heat, which is one of the main causes to the UHI effect. This explains the constant rising pattern between LST and %ISA.

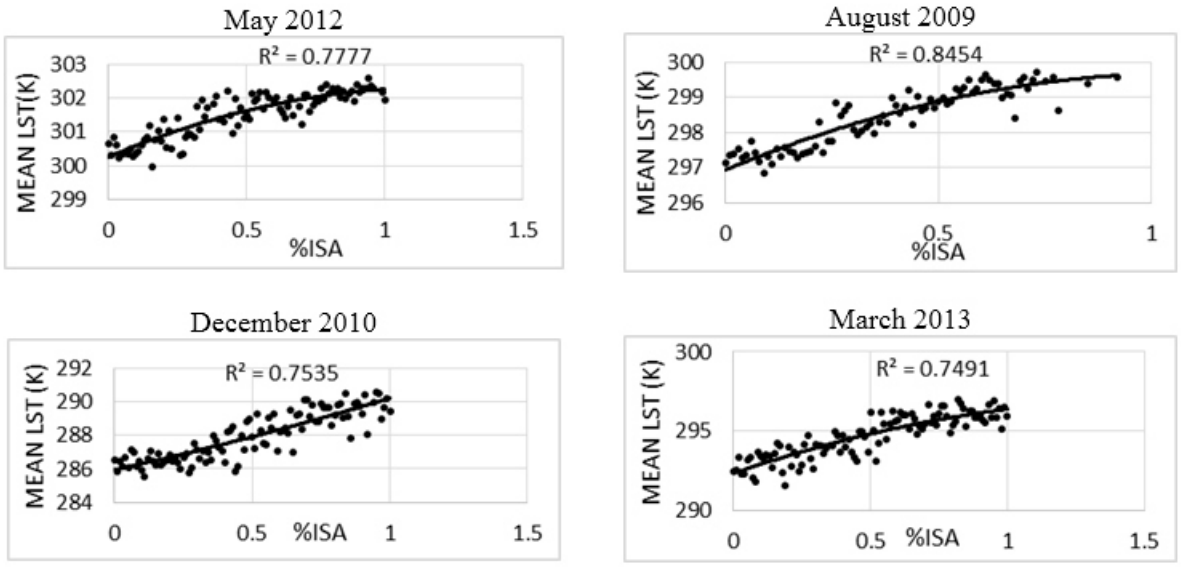

Figure 6 Mean LST and %ISA relationship for different seasons

Figure 6 shows the relationship between mean LST and %ISA for all seasons. Normally the graph correlating mean LST and %ISA shows rising trend in all seasons. The coefficient of correlation during monsoon season shows higher values compared to winter and summer season.

5. CONCLUSIONS

Eight-day night time LST has been utilized in the present study, for the analysis of UHI effect of Ahmedabad city in India , which has been undertaken for summer, monsoon and winter seasons. Significant SUHI has been observed in the study area from the analysis of five years LST data from 2009 to 2013. Central part of the Ahmedabad city is extreme hot compared to other part of the city because of large number of roads, complex infrastructure and high peak buildings. Most of the high temperature pixels fall within the urban boundary and LSTs of the urban area are higher as compared to LSTs of the area outside the urban boundary. In case of Ahmedabad study area, Minimum LSTs are observed over the area at the boundary of study area, especially on the Western side. LST of Eastern and Southern parts of the rural areas is higher than the LST of Western and Northern parts of rural areas. In the present study, urban parameter %ISA which represent the extend of urbanization has been used for the UHI analysis. Positive relationship has been found between LST and %ISA. The relationship between LST and %ISA is almost same throughout the entire season for the study area with a consistent rising trend. Though high variation can be observed in the scatter plots showing weak trend for low %ISA values but the trend is strong for high %ISA values. In the mean LST v/s %ISA relationship, it has been observed that the coefficient of correlation of monsoon season has been found to be higher compared to winter and summer seasons.

REFERENCES

Chander, G., & Markham, B. (2003). Revised Landsat-5 TM radiometric calibration procedures and post calibration dynamic ranges. IEEE Transactions on Geoscience and Remote Sensing, 41(11), 2674−2677.

Karl, T.R., Diaz H.F. & Kukla, G. (1988). Urbanization: Its detection and effect in the united states climate record. Journal of Climate, 1(11), 1099-1123.

LPDAAC (2010c). Land Surface Temperature & Emissivity 8-Day L3 Global 1km. USGS website, URL: https://lpdaac.usgs.gov/lpdaac/products/modis_products_table/land_surface_temperature_emissivity/8_day_l3_global_1km/myd11a2 (Accessed: June 2010)

LPDAAC (2011). Land Cover Type Yearly L3 Global 500 m SIN Grid available online at)

Mathew. A, Chaudhary. R, Gupta. N, Khandelwal. S & Kaul. N (2015), Study of Urban Heat Island Effect on Ahmedabad City and Its Relationship with Urbanization and Vegetation Parameters. International Conference on Emerging Trends of Engineering, Science, Management and its Applications (ICETESMA-15), 560-567.

NASA, 2008. Landsat 7 Science Data Users Handbook. http://landsathandbook.gsfc.nasa.gov/handbook.html, (accessed 25 Feb. 2008).

Oke, T.R. (1982). The energetic basis of the urban heat island. Quarterly Journal of the Royal Meteorological Society, 108, 1–24.

Owen, T.W., Carlson, T.N. & Gillies, R.R. (1998). An assessment of satellite remotely-sensed land cover parameters in quantitatively describing the climatic effect of urbanization. International Journal of Remote Sensing, 19, 1663-1681.

Voogt, J.A., & Oke, T.R. (2003). Thermal remote sensing of urban climates. Remote Sensing of the Environment, 86, 370–384.

Weng, W.C., Zeng, Z. & Karl, T.R. (1990). Urban heat islands in China. Geophysical Research Letters, 17(12), 2377-2380.

Yuan, F., & Bauer, M.E. (2007). Comparison of impervious surface area and normalized difference vegetation index as indicators of surface urban heat island effects in Landsat imagery, Remote Sensing of Environment, 106, 375-386.

Zhang, K., Wang, R., Shen, C. & Da, L. (2010). Temporal and spatial characteristics of the urban heat island during rapid urbanization in Shanghai, China. Environmental Monitoring and Assessment, 169, 101-112.

Zhang, Y., Odeh, I.O.A. & Han, C. (2009). Bi-temporal characterization of land surface temperature in relation to impervious surface area, NDVI and NDBI, using sub-pixel image analysis. International Journal of Applied Earth Observation and Geoinformation, 11, 256-264.

Erosion Risk Estimation of Alaknanda River Basin Using Morphometric Indices

Sugandha Panwar[1], Govind Joseph Chakrapani[2]
[1,2]Department of Earth Sciences,
Indian Institute of Technology Roorkee, Roorkee, India-247667
Email: sugandha.panwar@gmail.com

ABSTRACT

The Himalayan watersheds are featured by active tectonics and high climatic variability. River Ganga that carries the highest suspended sediment load in the world is supported by two headwater streams namely the Alaknanda and Bhagirathi River. Alaknanda River supplies large amount of sediment and dissolved load to river Ganga. During the monsoon season, the physical erosion rate in the Alaknanda river basin is quite high. Due to mountainous physiography and perennial hydrologic conditions, the basin offers huge hydropower potential. The biggest challenge for the hydropower generation is the sediment load carried by the river. Sediment load directly depends on the erosion activities in the basin. In the absence of hydrological and meteorological data, geomorphic evaluation provides a reliable approach to study erosion risk estimation at a basin scale. The present study aims to estimate the erosion potential of the sub-catchment areas of the Alaknanda River through morphometric indices. Using geographic information system as a tool, six sub-catchment areas were extracted namely Alaknanda main channel (AMC), Mandakini, Pinder, Nandakini, Birahi Ganga and Dhauli Ganga and in total 22 morphometric parameters were calculated. The result shows that factors such as basin shape, relief, drainage density and stream frequency supports the high erosion activities in the Alaknanda basin. The study is important as it classifies erosion vulnerability of sub-watersheds of the Alaknanda basin that are facing environmental degradation due to many hydropower project constructions.

Keywords—Alaknanda Basin, Morphometric Indices, Drainage Density, Bifuration Ratio

1. INTRODUCTION

The Himalayas are characterized by high tectonic activities and heavy monsoon rainfall that makes the region prone to natural disasters such as earthquakes, floods and landslides. The Alaknanda river basin that lies in the Western Himalayan region of India is highly prone to flash floods and landslides (Fig. 1 shows the location of the Alaknanda river basin). Physiographically, the area consists of structural hills, valley, terraces, glaciers and piedmonts (Shukla et al. 2014). The Alaknanda River and its main tributaries (Mandakini, Pinder, Nandakni, Birahi Ganga and Dhauli Ganga) are all perennial in nature. The runoff in the rivers is controlled by both the glacial melt and rainfall events. During the monsoon months from June to September, ~75% of the annual rainfall is reported that increases the river discharge (Chakrapani and Saini 2009). Almost every year during the monsoon season, instances of flash floods and landslides are reported in the Alaknanda basin. A combination of natural events such as heavy precipitation, high temperature (resulting in snowmelt) and physiography of basin promotes high

high erosion activities in the basin. The physical erosion rate in the Alaknanda basin as reported by Chakrapani and Saini (2009) is 907 ton km2 yr-1 which is far in excess of the global average of 156 ton km2 yr-1. Due to its physiography and hydrologic conditions, the basin offers a huge hydropower potential. A number of dams and reservoirs are under operation and under construction. Remote Sensing and GIS techniques offer a quantitative measure to study the geomorphological features of the study area. Linear, areal and relief characteristics are measured that influence the hydrological response and erosion processes in the basin.

2. STUDY AREA

The study was carried out in the Alaknanda river basin that lies in the Western Himalayan region of India. Figure 1 shows the location of the Alaknanda river basin. Alaknanda River is a headwater stream of river Ganga and is a major contributor of sediment and dissolved load to it. The total catchment area of the Alaknanda basin is ~8716 Km2. Major tributaries of the Alaknanda river are Mandakini, Pindar, Nandakini, Birahi Ganga and Dhauli Ganga. All these tributaries are perennial in nature and flow through varied lithologies comprising of gneiss, granites, migmatites, schist, quartzites, limestone and slates (Valdiya 1980). The immense neotectonic activities have shaped the physiography of the basin, which comprises of high relief, steep slopes and high drainage density (Shukla et al. 2014). Approximately 75% of the annual rainfall occurring during the monsoon season (June-September) leads to high flow in these rivers (Chakrapani and Saini 2009). Due to heavy rains, high temperature and narrow valleys, instances of cloud burst, flash floods and landslides are very common in the Alaknanda basin. At the mouth of the watershed (Devprayag), Alaknanda River is of 10th order (Strahler number). In terms of land cover, ~60% of the watershed is covered by forest and ~21% of the land area is occupied by the glaciers. Though population density is quite less in the basin; anthropogenic presence is marked by the construction of dams, reservoirs and roads. According to South Asian Network on Dams River and Public (SANDRP), approximately 140 dams are under construction and under a proposal to fetch the hydropower from the Alaknanda and Bhagirathi river systems.

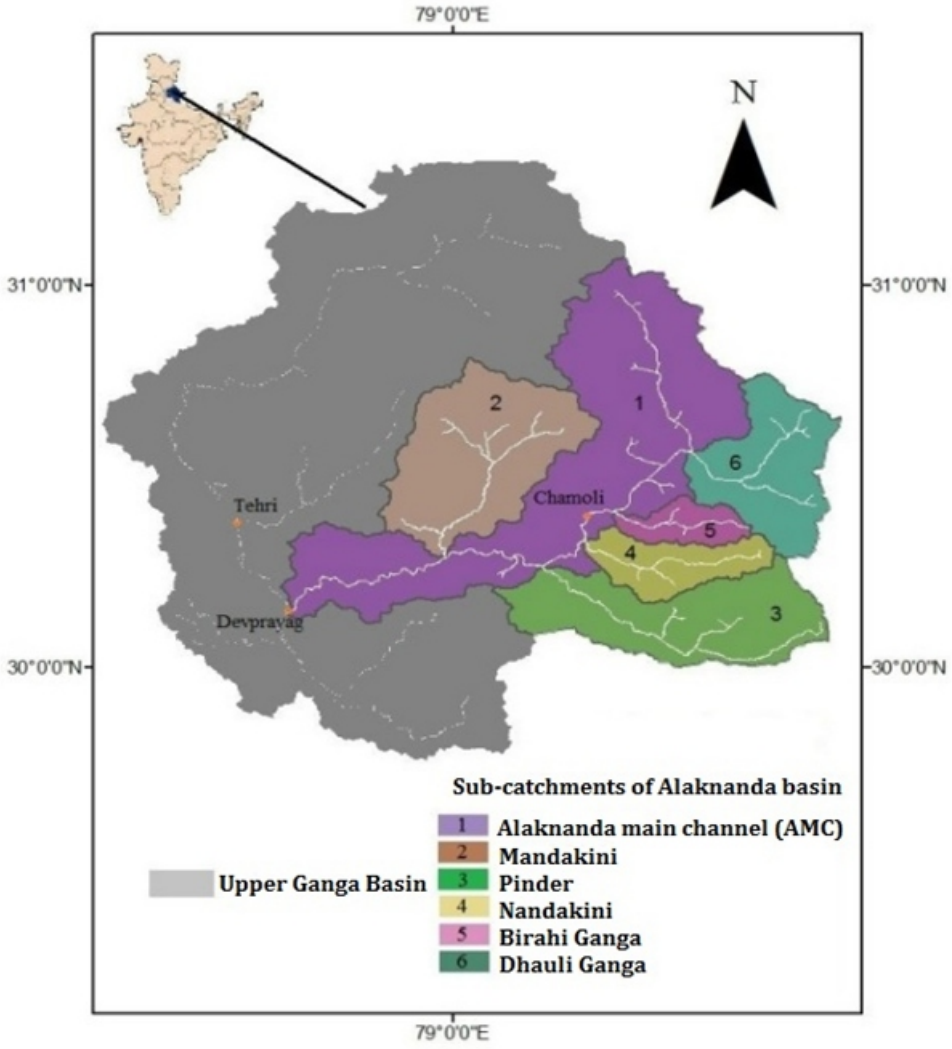

Figure 1 Study area location showing sub-catchment areas of the Alaknanda basin

3. METHODOLOGY

Remote Sensing and GIS technique offers a reliable tool to evaluate the risk of flood occurrence and erosion potential of the basin. In order to better understand the factors that promote high erosion in the Alaknanda basin, six sub-watersheds namely Alaknanda main channel (AMC), Mandakini, Pinder, Nandakini, Birahi Ganga and Dhauli Ganga River were extracted. Hydrological conditions and erosion risk was estimated individually for these watersheds (Fig. 1). SRTM DEM (90m), topographic sheets and LISS III satellite imagery of the year 2011 were used to evaluate the geomorphic indices. Table 1 shows the list of morphometric parameters calculated and the approach followed to calculate these parameters. In total 22 parameters were calculated. The spatial analyst tool in ARCGIS 10.1 was used to extract parameters such as slope, drainage density, catchment area, basin length, relief, etc. The erosion risk estimation was evaluated for each sub-watershed extracted (as shown in Fig. 1).

Table 1 Morphometric parameters calculated

Morphometric parameters		Symbol	Method/Reference
Linear	Stream Order	Os	(Strahler 1964)
	Channel Length	Lc	(Horton 1945)
	Bifuration Ratio	Br	(Horton 1945)
Basin	Basin Area (Km)	A	GIS application
	Basin Perimeter (Km)	P	GIS application
	Basin Length (Km)	Lb	GIS application
	Shape Factor	Sf	(Horton 1945)
	Elongation Ratio	Er	(Horton 1945)
	Drainage Texture	Dt	(Horton 1945)
	Circulatory Ratio	Cr	(Miller 1953)
	Compactness Coefficient	Cc	(Horton 1945)
Drainage	Stream Frequency	Fs	(Horton 1945)
	Drainage Density	Dd	(Strahler 1964)
	Total Stream Number	TS	GIS application
	Channel Gradient	Gc	GIS application
	Overland Flow	Of	(Horton 1945)
Relief	Basin Relief (m)	R	GIS application
	Ruggedness Number	Rn	(Strahler 1964)
	Slope (Degree)	S	GIS application
	Relief Ratio	Rr	(Vittala et al. 2004)
	Relief Peakedness	Rp	(Miller 1953)
	Geometry Number	Gn	(Horton 1945)

4. RESULTS AND DISCUSSION

Based on the approach proposed by Horton (1945), Sthaler (1952), Miller (1960), Vittala et al. (2004), Vijith and Satheesh (2006) and Shukla et al. (2014), morphometric analysis was carried out in all the six extracted sub-catchment areas of the Alaknanda basin. The value of each parameter is shown in table 2.

4.1. Morphometric Parameters

4.1.1. Linear Parameters

Important linear parameters calculated include stream order (Os), channel length (Lc) and bifurcation ratio (Br). Stream order (Os) is an important parameter that expresses the hierarchy of individual river segment (Strahler 1964). Table 2 shows the stream order value of each stream. High Os indicates high contribution of water to the main channel. In all the sub-catchments, first order streams possess maximum length. It was observed that as the Os increases, length of streams does not decrease highlighting the effect of varied lithology and structural disturbance in the region. On the eastern side, four major sub-watersheds (Birahi Ganga, Pinder, Nandakini, and Dhauli Ganga) are present that have 7th, 8th and 9th order streams, whereas, on the western side only Mandakini watershed is present.

Presence of large stream numbers (Os) and stream length (Lc) on the eastern side of Alaknanda basin makes the eastern part of the basin more vulnerable to fluvial erosion. Similar to the pattern shown by stream order, the high bifurcation ratio in the Nandakini, Birahi Ganga and Dhauli Ganga indicates the dominance of structural control and lithological complexity (Vijith and Satheesh 2006; Pareta and Pareta 2011; Shukla et al. 2014). Active thrust zones- Main Central Thrust (MCT) and STDS (South Tibetan Detachment System) pass through this zone that influences the structural stability of the area promoting landslides, earthquakes and avalanches.

Table 2 Morphometric parameters for the sub-watersheds of Alaknanda basin

	Sub-watersheds					
Parameter	**AMB**	**Mandakini**	**Pinder**	**Nandakini**	**Birahi Ganga**	**Dhauli Ganga**
	-1	**-2**	**-3**	**-4**	**-5**	**-6**
Os	10	9	8	8	7	9
Lc	202.8	67	88	49	32	53
Br	2.5	2.3	2.1	36.9	31.1	17.2
A	3657	1645	1489	547	297	1082
P	170	202	225	122	97	170
Lb	128.5	58.1	70.4	44.2	31.9	41.8
Fs	4.5	2.1	3.3	3.5	3.4	1.6
Er	0.3	0.3	0.3	0.3	0.3	0.5
Dt	9.9	10.8	10.1	7.4	5.8	9.2
Cr	0.2	0.5	0.4	0.4	0.004	0.5
Cc	2.2	1.4	1.6	1.5	1.5	1.5
Fs	1.3	1.3	1.5	1.7	1.7	1.4
Dd	1.114	0.776	0.86	0.974	0.649	0.974
TS	4759	2179	2270	937	531	1570
Gc	33.9	43.9	18.3	61.4	86.4	47.1
Of	0.03	0.03	0.03	0.03	0.03	0.03
R	7005	6121	5664	6034	5022	5704
Rn	54.6	49.9	47	51.4	52.6	54.1
S	28.9	29.4	29.4	30.5	33.6	33
Rr	56.5	105.4	80.4	136.6	157.3	136.4
Rp	0.5	0.5	0.5	0.5	0.5	0.6
Gn	1.9	1.7	1.6	1.7	1.6	1.7

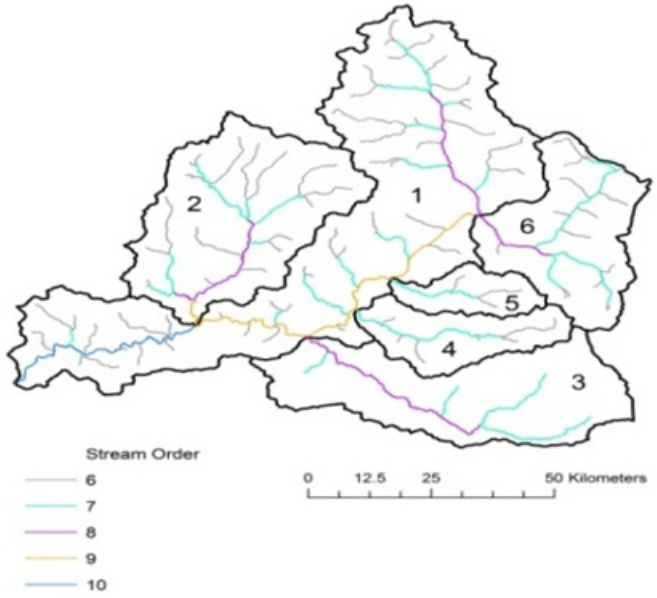

Figure 2 Stream order in sub-watershed of Alaknanda Basin

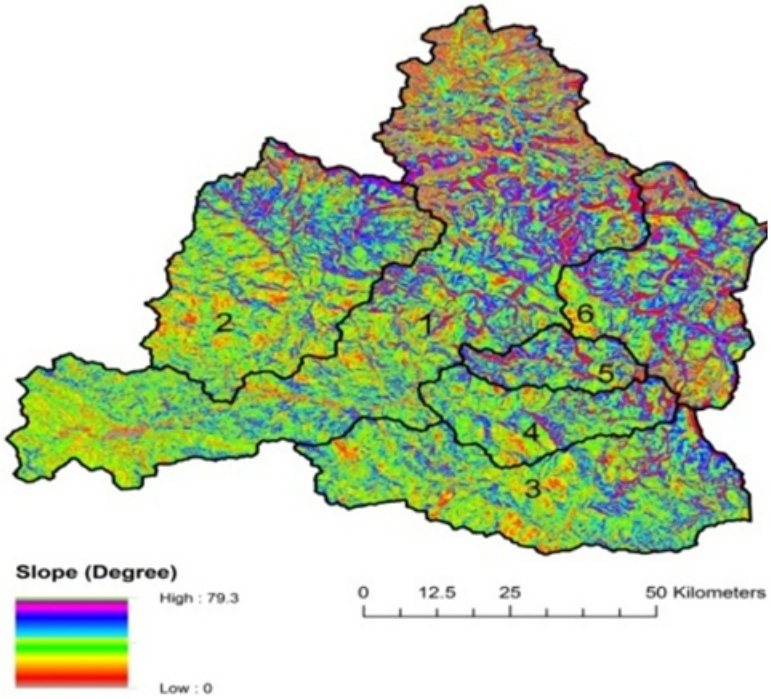

Figure 3 Slope map of sub-watersheds of Alaknanda Basin

4.1.2. Basin Parameter

The parameters such as shape factor (Sf), elongation ratio (Er), circularity ratio (Cr), and compactness coefficient (Cc) gives an idea about the circularity of the basin (Horton 1945; Schumms 1956; Vijith and Satheesh 2006; Shukla et al. 2014). The circular character of the basin indicates shorter lag time to reach peak flow. Table 2 shows the computed value of the basin parameters. The results show all the extracted watersheds are elongated in shape with high relief and steep slopes. Drainage texture (Dt) points out that

the stream texture is very fine in nature which indicates that they have smaller lag time leading to peak discharge and supports high erosion in the Alaknanda basin.

4.1.3. Drainage Parameter

Stream frequency (Sf) is related to permeability, infiltration capacity, and relief of the watershed. Structurally controlled basin shows high stream frequency and high drainage density. The high value of Sf for Birahi Ganga and Alaknanda main channel (AMC) points that the catchment area comprises of rocky terrain with low infiltration capacity. Drainage density (Dd) varies from 0.65 to 1.11 (Fig. 2). Birahi Ganga shows the greatest basin lag time. Overland flow (Of) is also an important parameter that influences both the hydrology and physiography of the basin. It is calculated as one half of the reciprocal of the drainage basin (Horton 1945). This value indicates that in all the watersheds, runoff will be very fast due to steep slopes.

4.1.4. Relief Parameter

Relief parameters such as relief ratio (Rr), relief peakedness (Rp) and geometry number (Gn) mentioned in table 1 indicate that Alaknanda basin is featured by high relief and steep slopes that leads to shorter lag time (Fig. 3). The values of ruggedness number and geometry number indicate soil erosion is quite high in the Alaknanda main stream sub-catchment, whereas, minimum soil erosion is present in the Birahi Ganga watershed (Schumms 1956).

5. CONCLUSION

Based on the derived morphometric parameters, it is seen that erosion intensity is quite high on the eastern side of Alaknanda basin. High values of stream order, drainage density and bifurcation ratio indicate the dominance of structural control and lithological complexity. The high value of stream frequency points that the catchment area comprises of rocky terrain with low infiltration capacity. Elongation ratio shows the area is marked with high relief and steep slopes indicating shorter lag time exists for the peak flow. Among all the sub-watersheds extracted, Birahi Ganga shows the greatest basin lag time. Overland flow and relief indices also indicate that in all the watersheds, runoff will be very fast due to steep slopes. The values of ruggedness number and geometry number indicate soil erosion is quite high in the Alaknanda main stream sub-catchment, whereas, minimum soil erosion is present in the Birahi Ganga watershed.

REFERENCES

Chakrapani, G. J., Saini, R. K. (2009). Temporal and spatial variations in water discharge and sediment load in the Alaknanda and Bhagirathi Rivers in Himalaya, India. Journal of Asian Earth Sciences, 35, 545-553.

Horton, R. E. (1945). Erosional development of streams and their drainage basins: Hydrophysical approach to quantitative morphology. Geological Society of America Bulletin, 56, 275-370.

Miller, V.C. (1953). A quantitative geomorphic study of drainage basin characteristics in the Clinch mountain area, Virginia and Tennessee. Technical Report 3 NR 389-402, Columbia University, Department of Geology, ONR, New York, USA.

Pareta, K., Pareta, U. (2011). Quantitative morphometric analysis of a watershed of Yamuna basin, India using ASTER (DEM) data and GIS. International Journal of Geomatics and Geosciences, 2(1), 41-56.

Schumms, S. A. (1956). Evolution of drainage systems and slopes in Badlands at Perth Amboy, New Jersey. Bulletin of the Geological Society of America, 67, 597-646.

Shukla, D. P., Dubey, C. S., Ningreichon, N. S., Singh, R. P., Mishra, B. K., Singh, S. K. (2014). GIS-based morpho-tectonics study of Alaknanda basin: a precursor for hazard zonation. Natural Hazards, 71, 1433-1452.

Strahler, A. (1964). Quantitative geomorphology of drainage basins and channel networks, Handbook of Applied Hydrology. V.T. Chow Ed., section 4-11, McGraw-Hill New York, USA.

Valdiya, K. S. (1980). Geology of Kumaun Lesser Himalaya. Wadia Institute of Himalayan Geology, Dehradun, pp. 291.

Vijith, H., R. Satheesh, R. (2006). GIS based morphometric analysis of two major upland sub-watersheds of Meenachil River in Kerala. Journal of the Indian Society of Remote Sensing, 34(2), 181-185.

Vittala S. S., Govindaiah, S., Honne G. H. (2004). Morphometric analysis of sub-watersheds in the Pavagada area of Tumkur district, South India using remote sensing and GIS techniques. Journal of Indian Society of Remote Sensing, 32(4), 351-362.

Instructions for Authors

Essentials for Publishing in this Journal

1 Submitted articles should not have been previously published or be currently under consideration for publication elsewhere.

2 Conference papers may only be submitted if the paper has been completely re-written (taken to mean more than 50%) and the author has cleared any necessary permission with the copyright owner if it has been previously copyrighted.

3 All our articles are refereed through a double-blind process.

4 All authors must declare they have read and agreed to the content of the submitted article and must sign a declaration correspond to the originality of the article.

Submission Process

All articles for this journal must be submitted using our online submissions system. http://enrichedpub.com/ . Please use the Submit Your Article link in the Author Service area.

-

Manuscript Guidelines

The instructions to authors about the article preparation for publication in the Manuscripts are submitted online, through the e-Ur (Electronic editing) system, developed by **Enriched Publications Pvt. Ltd**. The article should contain the abstract with keywords, introduction, body, conclusion, references and the summary in English language (without heading and subheading enumeration). The article length should not exceed 16 pages of A4 paper format.

Title

The title should be informative. It is in both Journal's and author's best interest to use terms suitable. For indexing and word search. If there are no such terms in the title, the author is strongly advised to add a subtitle. The title should be given in English as well. The titles precede the abstract and the summary in an appropriate language.

Letterhead Title

The letterhead title is given at a top of each page for easier identification of article copies in an Electronic form in particular. It contains the author's surname and first name initial .article title, journal title and collation (year, volume, and issue, first and last page). The journal and article titles can be given in a shortened form.

Author's Name

Full name(s) of author(s) should be used. It is advisable to give the middle initial. Names are given in their original form.

Contact Details

The postal address or the e-mail address of the author (usually of the first one if there are more Authors) is given in the footnote at the bottom of the first page.

Type of Articles

Classification of articles is a duty of the editorial staff and is of special importance. Referees and the members of the editorial staff, or section editors, can propose a category, but the editor-in-chief has the sole responsibility for their classification. Journal articles are classified as follows:

Scientific articles:

1. Original scientific paper (giving the previously unpublished results of the author's own research based on management methods).

2. Survey paper (giving an original, detailed and critical view of a research problem or an area to which the author has made a contribution visible through his self-citation);

3. Short or preliminary communication (original management paper of full format but of a smaller extent or of a preliminary character);

4. Scientific critique or forum (discussion on a particular scientific topic, based exclusively on management argumentation) and commentaries. Exceptionally, in particular areas, a scientific paper in the Journal can be in a form of a monograph or a critical edition of scientific data (historical, archival, lexicographic, bibliographic, data survey, etc.) which were unknown or hardly accessible for scientific research.

Professional articles:

1. Professional paper (contribution offering experience useful for improvement of professional practice but not necessarily based on scientific methods);
2. Informative contribution (editorial, commentary, etc.);
3. Review (of a book, software, case study, scientific event, etc.)

Language

The article should be in English. The grammar and style of the article should be of good quality. The systematized text should be without abbreviations (except standard ones). All measurements must be in SI units. The sequence of formulae is denoted in Arabic numerals in parentheses on the right-hand side.

Abstract and Summary

An abstract is a concise informative presentation of the article content for fast and accurate Evaluation of its relevance. It is both in the Editorial Office's and the author's best interest for an abstract to contain terms often used for indexing and article search. The abstract describes the purpose of the study and the methods, outlines the findings and state the conclusions. A 100- to 250-Word abstract should be placed between the title and the keywords with the body text to follow. Besides an abstract are advised to have a summary in English, at the end of the article, after the Reference list. The summary should be structured and long up to 1/10 of the article length (it is more extensive than the abstract).

Keywords

Keywords are terms or phrases showing adequately the article content for indexing and search purposes. They should be allocated heaving in mind widely accepted international sources (index, dictionary or thesaurus), such as the Web of Science keyword list for science in general. The higher their usage frequency is the better. Up to 10 keywords immediately follow the abstract and the summary, in respective languages.

Acknowledgements

The name and the number of the project or programmed within which the article was realized is given in a separate note at the bottom of the first page together with the name of the institution which financially supported the project or programmed.

Tables and Illustrations

All the captions should be in the original language as well as in English, together with the texts in illustrations if possible. Tables are typed in the same style as the text and are denoted by numerals at the top. Photographs and drawings, placed appropriately in the text, should be clear, precise and suitable for reproduction. Drawings should be created in Word or Corel.

Citation in the Text

Citation in the text must be uniform. When citing references in the text, use the reference number set in square brackets from the Reference list at the end of the article.

Footnotes

Footnotes are given at the bottom of the page with the text they refer to. They can contain less relevant details, additional explanations or used sources (e.g. scientific material, manuals). They cannot replace the cited literature.
The article should be accompanied with a cover letter with the information about the author(s): surname, middle initial, first name, and citizen personal number, rank, title, e-mail address, and affiliation address, home address including municipality, phone number in the office and at home (or a mobile phone number). The cover letter should state the type of the article and tell which illustrations are original and which are not.

Address of the Editorial Office:

Enriched Publications Pvt. Ltd.
S-9,IInd FLOOR, MLU POCKET,
MANISH ABHINAV PLAZA-II, ABOVE FEDERAL BANK,
PLOT NO-5, SECTOR -5, DWARKA, NEW DELHI, INDIA-110075,
PHONE: - + (91)-(11)-45525005

Notes: